Alkaline Earth-centered CO Homologation, Reduction and Amine Carbonylation

Mathew D. Anker,[a] Christos E. Kefalidis,[b] Yan Yang,[c] Jian Fang,[c] Michael S. Hill,[a,*] Mary F. Mahon[a,d*] and Laurent Maron[b,*]

[a] *Department of Chemistry, University of Bath, Claverton Down, Bath, BA2 7AY, UK*

[b] *Université de Toulouse et CNRS, INSA, UPS, UMR 5215, LPCNO, 135 Avenue de Rangueil, F-31077 Toulouse, France*

[c] *Key Laboratory of Nonferrous Metal Chemistry and Resources Utilization of Gansu Province School of Chemistry and Chemical Engineering, Lanzhou University, Lanzhou 730000, PR China.*

[d] *X-ray Crystallographic Suite, Department of Chemistry, University of Bath, Claverton Down, Bath, BA2 7AY, UK.*

Email: msh27@bath.ac.uk

Abstract

Reactions of *β*-diketiminato magnesium and calcium hydrides with 1 atmosphere of CO result in a reductive coupling process to produce the corresponding derivatives of the *cis*-ethenediolate dianion. Computational (DFT) analysis of this processes mediated by Ca, Sr and Ba highlight a common mechanism and a facility for the reaction that increases with increasing alkaline earth (Ae) atomic weight. Reaction of CO with $PhSiH_3$ in the presence of the magnesium or calcium hydrides results in catalytic reduction to methylsilane and methylene silylether products, respectively. These reactions are proposed to ensue via the interception of initially formed group 2 formyl intermediates, an inference which is confirmed by a DFT analysis of the magnesium-centered reaction. The computational results identify the rate determining process, requiring traversal of a 33.9 kcal mol^{-1} barrier, as a Mg-H/C-O σ-bond metathesis reaction, to be associated with the ultimate cleavage of the C-O bond. The carbonylation reactivity is extended to a variety of magnesium and calcium amides. With primary amido complexes, which for calcium include a derivative of the parent $[NH_2]^-$ anion, CO insertion is facile and ensues with subsequent nitrogen-to-carbon migration of hydrogen to yield a variety of dinuclear and, in one case, trinuclear formamidate species. The generation of initial carbamoyl carbenic intermediates is strongly implicated through the isolation of the CO insertion product of a magnesium *N*-methylanilide derivative. These observations are reinforced by a DFT analysis of the calcium-centred reaction with aniline, which confirms the exothermicity of the formamidate formation ($\Delta H = -67.7$ kcal mol^{-1}). Stoichiometric reduction

of the resultant magnesium and calcium formamidates with pinacolborane results in the synthesis of the corresponding *N*-borylated methylamines. This takes place via a sequence of reactions initiated through the generation of amidatohydridoborate intermediates and a cascade of reactivity that is analogous to that previously reported for the deoxygenative hydroboration of organic isocyanates catalysed by the same magnesium hydride pre-catalyst. Although a sequence of amine formylation and deoxygenation may be readily envisaged for the catalytic utilization of CO as a C_1 source in the production of methylamines, our observations demonstrate that competitive amine-borane dehydrocoupling is too facile under the conditions of 1 atmosphere of CO employed.

Introduction

The carbonylation of organic molecules with carbon monoxide underpins some of the most widely employed chemical processes.[1-4] For the best part of a century the development of, for example, olefin hydroformylation,[5-12] stoichiometric and catalytic Pauson-Khand reactivity[13, 14] and the heterogeneous conversion of CO/dihydrogen mixtures to liquid hydrocarbon fuels through Fischer-Tropsch chemistry have motivated intense interest in the reactivity of carbon monoxide at typical mid-to-late transition metal centers.[15-17] As a consequence, the chemistry of metal carbonyl derivatives and the reactivity of later transition metal species toward CO are some of the best understood processes in organometallic chemistry. In contrast, reports of CO addition to the polar M-X (X = e.g. C, N, H) bonds of more electropositive and redox-inactive early transition metal or 4f-element species have been more sporadic.[18-20] Of most relevance to the current work, a handful of reports have shown that treatment of zirconium(IV), cerium(III) and samarium(III) hydride species with CO allows the preparation of ethenediolate derivatives such as species **1** – **3** (Chart 1).[21-28] While the formation of these compounds demonstrates that homologation and reductive coupling of CO may be achieved at a group 4 or lanthanide center, it is notable that no onward or further productive reactivity has been described.

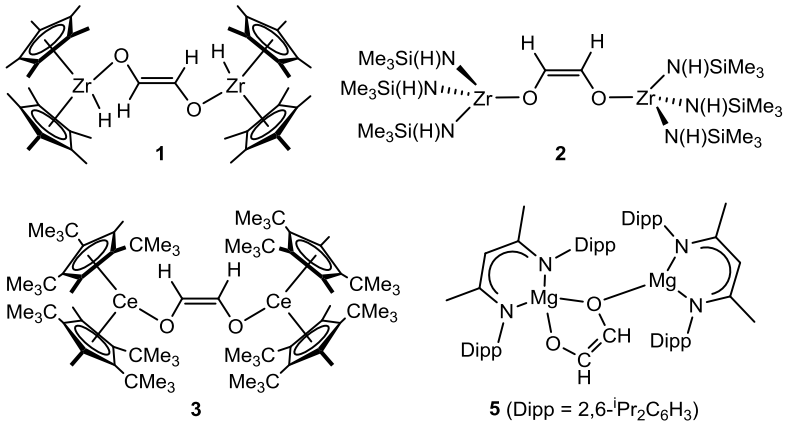

Chart 1: Examples of previously described ethenediolate derivatives assembled from CO at d^0 metal centers.

The reactivity of lithium alkyls and amides with carbon monoxide has been a subject of study for over a century, albeit the electrophilic trapping of the resultant acyl or carbamoyl anion equivalents has only been achieved infrequently.[29-41] Related chemistry induced by organo- or amidomagnesium derivatives has received even less attention, despite the possibility that the reduced nucleophilicity of the resultant species may provide greater selectivity in subsequent transformations.[42] Prompted by this lacuna, we have recently reported that the reaction of the β-diketiminato magnesium hydride $[HC\{(Me)CNDipp\}_2MgH]_2$ (**4**, Dipp = 2,6-di-

*iso*propylphenyl) with 1 atmosphere of CO results in the production of the *cis*-ethenediolate species (**5**).[43] The observation of a heavily deshielded doublet of doublets signal at δ 358.9 ppm during *in situ* low temperature (–90 °C) ^{13}C NMR experiments, led us to suggest that the homologation of two CO molecules had been achieved through the formation of an initial carbenic formyl intermediate (**6**) and the subsequent sequence of intramolecular hydrogen transfer and, via the oxomethylene species (**7**), further CO insertion illustrated in Scheme 1. Under this regime, the *cis* stereochemistry of the ethenediolate dianion is enforced by the anti-periplanar orientation of the C-H bonds to the carbon lone pair across the further carbenic intermediate (**8**). Compound **5** was reported simultaneously, and characterized as a mono THF adduct, by Jones, Maron and co-workers who also confirmed the exothermicity of the reaction sequence shown in Scheme 1 ($\Delta H = -82.9$ kcal mol^{-1}) through a computational analysis using density functional theory (DFT).[44] Consistent with the apparent facility of the reaction, these latter calculations demonstrated that **6** – **8** populate a shallow potential energy surface with a maximum barrier height of only 14.9 kcal mol^{-1} associated with the ultimate transformation of **8** to **5**.

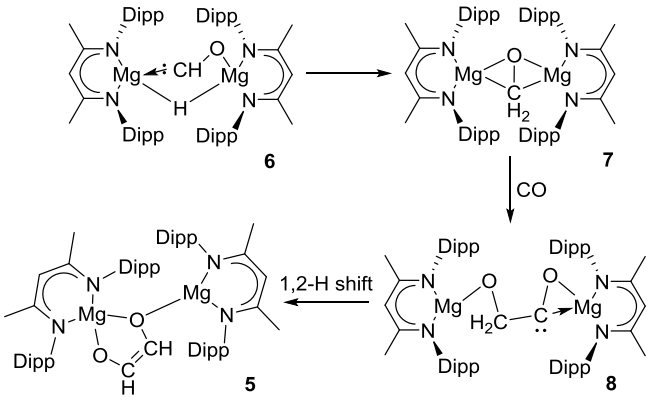

Scheme 1: Experimentally deduced mechanism for the formation of compound **5**.

The potential of this chemistry for the development of homologative and reductive processes reminiscent of Fischer-Tropsch catalysis was highlighted through Jones' further isolation of a trimeric magnesium derivative of the κ^3-$\{C_3(H_3)O_3\}^{3-}$ trianion and our own demonstration that CO could be reduced under very mild conditions (60 °C, 1 atm. CO) to the methyl silane, PhH_2SiCH_3, by $PhSiH_3$ in the presence of catalytic quantities of compound **4**.[43, 44] This latter reactivity was suggested to ensue through the effective interception of carbenic intermediates such as **6**, with subsequent deoxygenation predicated on a sequence of rapid and unobservable C=O/Mg-H and Mg-O/Si-H metathesis events driven by the production of stable siloxane by-products.

In this contribution we present a combined synthetic and computational (DFT) study which extends this stoichiometric and catalytic CO homologation and reduction chemistry to calcium and exploits the carbonylation of alkaline earth (Ae) amides for the synthesis of *N*-alkyl and *N*-aryl formamide derivatives. Furthermore, we demonstrate that these latter species may be reduced to provide methylamine products enabling the, to the best of our knowledge, first selective exploitation of carbon monoxide as a C_1 synthon in the homogeneous synthesis of small nitrogenous organic molecules.

Results and Discussion

In an attempt to identify further intermediates during the magnesium-centered reductive coupling of CO, the *β*-diketiminato magnesium hydride [HC{(*t*-Bu)CNDipp}$_2$MgH]$_2$ (**9**) was reacted with one atmosphere of ^{13}CO at −90 °C.[45] Although the increased steric protection provided by the *tert*-butylated *β*-diketiminate ligand to magnesium was anticipated to retard of the rate of reaction and allow observation of further intermediate species analogous to **7** and **8**, monitoring of the reaction by ^{1}H and ^{13}C NMR spectroscopy indicated the generation of only a single new compound (**10**) within the first point of analysis (Scheme 2). Compound **10** was characterized by diagnostic 10 line AA′XX′ patterns ($^1J_{CH}$ = 170.2, $^2J_{CH}$ = 24.9, $^1J_{CC}$ = 80.5, $^3J_{HH}$ = 0.7 Hz) in both the ^{1}H and ^{13}C-^{1}H gated NMR spectra, which were strongly reminiscent of the signals resulting from the carbon and hydrogen environments of the *cis*-ethenediolate ligand within the previously reported compound **5**.[43]

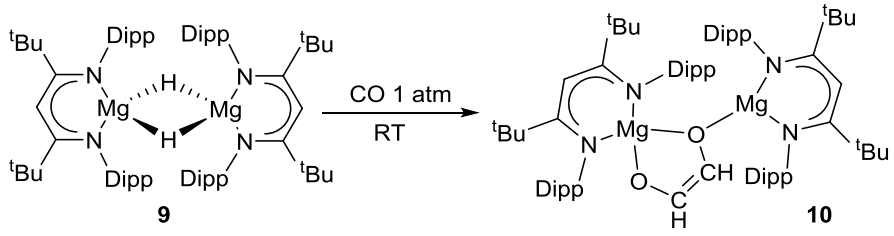

Scheme 2: Synthesis of compound **10**

Crystallization from the reaction solution at room temperature provided compound **10** as colorless blocks suitable for an X-ray diffraction analysis. The solid-state structure of **10** (Figure 1 and Table 1) demonstrates that the increased steric congestion of the magnesium center results in only limited structural modification in comparison to compound **5**. The *cis*-ethenediolate ligand again adopts a κ^2-μ_2-bridging mode between the respective four-coordinate Mg1 and three-coordinate Mg2 centers, which is analogous to that observed in **5**. Although there are some slight variations across the most relevant bond lengths and angles, the similarity of these species renders any further comment about the structure of **10** unnecessary.

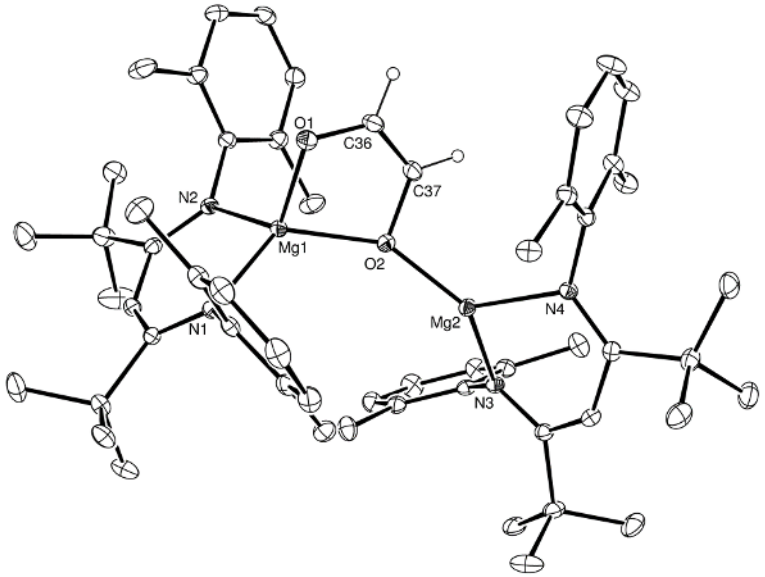

Figure 1: ORTEP representation of **10** (25% probability ellipsoids). Hydrogen atoms except those attached to C36 and C37 and *iso*-propyl methyl carbon atoms are removed for clarity. Selected bond lengths (Å) and angles (°): Mg1–O1 1.9207(10), Mg1–O2 2.0283(10), Mg1–N1 2.0505(11), Mg1–N2 2.0595(11), Mg2–O2 1.9067(10), Mg2–N4 2.0316(11), Mg2–N3 2.0157(11), C36–C37 1.328(2). O1–Mg1–O2 88.80(4), O1–Mg1–N1 119.06(5), O1–Mg1–N2 113.16(5), O2–Mg2–N3 136.76(5), O2–Mg2–N4 123.03(4), N3–Mg2–N4 98.68(5).

In a similar manner to the reactions performed with the magnesium hydrides, compounds **4** and **9**, a solution of the *β*-diketiminato calcium hydride, $[HC\{(Me)CNDipp\}_2CaH(THF)]_2$ (**11**),[46] in d_8-toluene immediately provided a single new species (**12**) when placed under one atmosphere of CO at room temperature. Compound **12** was characterized by the appearance of a singlet resonance at δ 5.00 ppm in its ^{1}H NMR spectrum with an accompanying vinylic carbon resonance at δ 134.9 ppm in the corresponding ^{13}C NMR spectrum. Repetition of this reaction with ^{13}CO afforded (**12**-^{13}C), which again provided AA′XX′ multiplet resonances ($^1J_{CH}$ = 180.9, $^2J_{CH}$ = 20.4, $^1J_{CC}$ = 61.6, $^3J_{HH}$ = 1.1 Hz) in both the ^{1}H and ^{13}C-^{1}H gated NMR spectra allowing the assignment of compound **12** as a calcium *cis*-ethenediolate derivative (Scheme 3).

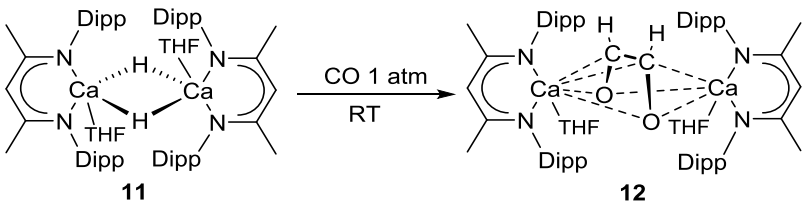

11 **12**

Scheme 3: Synthesis of compound **12**.

An X-ray diffraction analysis was performed on a single crystal of compound **12** grown from a saturated toluene solution (Figure 2). Details of the analysis and selected bond length and angle data are provided in Table 1 and the figure caption respectively. Compound **12** is a dimeric calcium species in which the two seven-coordinate calcium centers are bridged by a dianionic *cis*-ethenediolate ligand. The Ca1 and Ca2 centers are each further coordinated by a molecule of THF and the bidentate β-diketiminate ligands, which adopt an approximately orthogonal and mutually staggered disposition, presumably as a result of the steric demands of the bulky *N*-aryl substituents. In contrast to the asymmetric bridging mode adopted by the identical moiety in compounds **5** and **10**, the {O(1)-C(30)-C(31)-O(2)} *cis*-ethenediolate ligand bonds through symmetrically bridging η^4-interactions to each calcium center. This change in hapticity is most readily attributed to the larger ionic radius and greater polarizability of calcium (1.06 Å) in comparison to magnesium (0.78 Å).

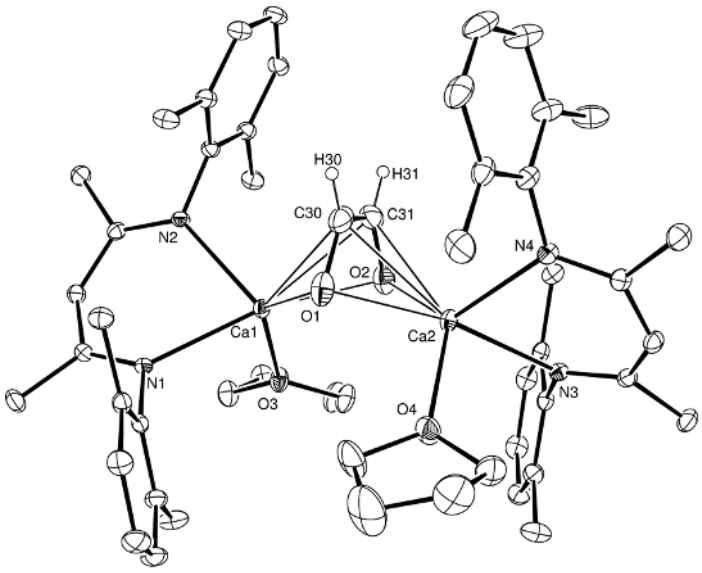

Figure 2: ORTEP representation of **12** (25% probability ellipsoids). Hydrogen atoms except H30 and H31 and *iso*-propyl methyl carbon atoms are removed for clarity. Selected bond lengths (Å) and angles (°): Ca1–O1 2.329(2), Ca1–O2 2.3558(19), Ca1–O3 2.3803(16), Ca1–N1 2.4126(18), Ca1–N2 2.3758(18), Ca1–C30 2.623(3), Ca1–C31 2.625(3), Ca2–O1 2.349(2), Ca2–O2 2.3505(19), Ca2–O4 2.3663(19), Ca2–N3 2.4028(18), Ca2–N4 2.3859(19), Ca2–C30 2.607(3), Ca2–C31 2.612(3), O1–C30 1.365(4), O2–C31 1.353(4), C30–C31 1.346(5). O2–Ca1–N1 167.26(7), O2–Ca1–N2 113.57(7), O1–Ca1–N1 106.89, O1–Ca1–N2 118.35(7), N1–Ca1–C30 127.62(9), N1–Ca1–C31 156.32(9), N2–Ca1–C30 96.59(8), N2–Ca1–C31 94.73(8), N2–Ca1–N1 78.96(6), O2–Ca2–N3 102.44(7), O2–Ca2–N4 128.38(7), O1–Ca2–N3 165.90(7), O1–Ca2–N4 114.77(7), N3–Ca2–C30 151.82(10), N3–Ca2–C31 122.74(9), N4–Ca2–N3 79.33(6), N4–Ca2–C30 99.77(8), N4–Ca2–C31 105.40(8), C31–C30–O1 119.2(3), C30–C31–O2 119.8(3).

Monitoring of the reaction between compound **11** and ^{13}CO in d_8-toluene at the low temperature limit of the solvent (–93 °C) by ^{1}H and ^{13}C NMR spectroscopy revealed only the formation of **12** and no evidence for the persistence of any calcium-containing intermediates analogous to compounds **6** – **8**. Similarly, addition of a single equivalent of CO by Toepler pump to the headspace of d_8-toluene solutions of compounds **4** and **11** in a J. Young NMR tube at either room temperature or –78 °C resulted in the consumption of only 50% of the hydride starting materials to provide compounds **5** and **12** respectively. These observations are consistent with the earlier calculations of Jones and Maron[44] and confirm that the onward reactivity with CO of both the initially formed products of hydridomagnesiation and hydridocalciation, the spectroscopically identified formyl-hydrido magnesium species **6** and a presumed analogous calcium derivative respectively, are extremely facile.

DFT calculations (B3PW91) were performed to provide a comparison between the relative facility of these magnesium- and calcium-mediated CO activation reactions along with the analogous reactions between CO and the, as yet hypothetical, β-diketiminato strontium and barium hydrides (Figure 3). Although there are some significant variations across the computed energies of the various heavier alkaline earth-derived intermediates and transition states, the computational study suggested the operation of a common mechanism, which is broadly analogous with that previously proposed for both the carbonylation of the magnesium hydride **4** (Scheme 1) and earlier f-block ethenediolate complexes. The hydride dimers react directly with one molecule of CO to give transient κ^2-C,O-formyl complexes, the C−O bonds of which further insert into the Ae−H bonds of the associated hydride fragments. The resultant dimeric oxomethylene compounds then react with a second molecule of CO through insertion into one of the Ae−C bonds and subsequent 1,2-hydrogen migration within the coordinated $C_2H_2O_2$ fragments provides the alkaline earth *cis*-ethenediolate complexes. The reactions are deduced to become marginally more exothermic with increasing alkaline earth atomic weight (ΔH = –82.9 (Mg);[44] –97.0 (Ca); –99.8 (Sr); –101.1 (Ba) kcal mol^{-1}) and our inability to observe a calcium-centered intermediate analogous to compound **6** during the reaction of compound **11** with CO is validated by the calculated barrier height of only 10.2 kcal mol^{-1}associated with the production of dimeric calcium oxomethylene intermediate. The onward reaction of this latter calcium species with CO is even more facile and, while the antiperiplanar 1,2-hydrogen transfer across the resultant carbenic intermediate is again deduced to be rate determining, the activation barrier associated with this process (18.4 kcal mol^{-1}) is only marginally higher than that calculated for the previously described magnesium-based process (14.9 kcal mol^{-1}).[44]

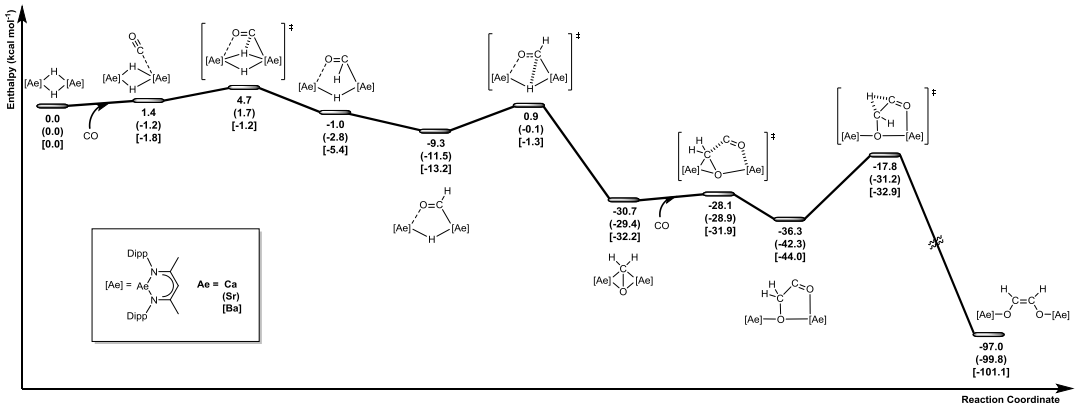

Figure 3: Computed (DFT, B3PW91) energy profiles for the formation of heavier alkaline earth *cis*-ethenediolate derivatives.

Catalytic Reduction of CO

In an attempt to observe homogeneous catalytic CO homologation and reduction analogous to the processes enabled by heterogeneous Fischer-Tropsch chemistry, d_8-toluene solutions of phenylsilane and 10 mol% of either compound **4** or **11** were exposed to 1 atmosphere of ^{13}CO and heated at 60 °C. The reaction employing **4** proved to be absolutely selective for the deoxygenative conversion of carbon monoxide to phenylmethylsilane (compound **14**, Scheme 4) and, although slow, requiring heating for 15 days to achieve 20% consumption of $PhSiH_3$ at 60 °C, provides the first example of any homogeneous main group-catalyzed reduction of CO to be described.

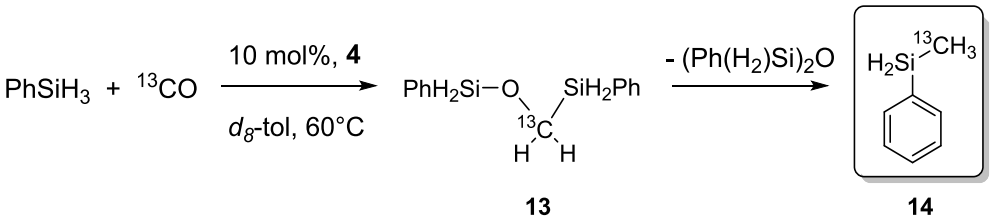

Scheme 4: Reduction of CO with phenylsilane as a hydride source, catalysed by **4**.

The formation of compound **14** was clearly evidenced through the development of a resonance at δ –7.32 ppm in the ^{13}C NMR spectrum, which appeared as a quartet of triplets ($^1J_{HC}$ = 122.0, $^3J_{HC}$ = 5.6 Hz) in the corresponding ^{13}C–^1H gated spectrum. Monitoring of these reactions by NMR spectroscopy also revealed the intermediacy of $Ph(H_2)Si$-O-$CH_2SiPh(H_2)$ (**13**). The methoxysilane (**13**) was clearly apparent through the observation of a resonance centered at 51.7 ppm in the ^{13}C NMR spectrum, which split as a binomial triplet of triplets signal ($^1J_{HC}$ =

130.7, $^{3}J_{HC}$ = 4.1 Hz) in the $^{13}C–^{1}H$ gated spectrum and was completely consumed at the cessation of the reaction.

The corresponding reaction utilizing the calcium hydride, compound **11**, provided a contrasting observation. This reaction was found to proceed at room temperature with almost complete consumption of the ^{13}CO atmosphere at the first point of analysis (within 60 minutes) to yield **13** as the sole ^{13}C-labelled product (Figure 4). No further reaction of compound **13** produced under these conditions could be observed, however, despite the addition of further equivalents of the $PhSiH_3$ hydride source. Rather, prolonged heating of the solution at 100 °C resulted in the apparent Schlenk redistribution of the calcium species to form the known and catalytically inactive homoleptic β-diketiminate derivative, [{HC{(Me)CNDipp}$_2$}$_2$Ca].[47]

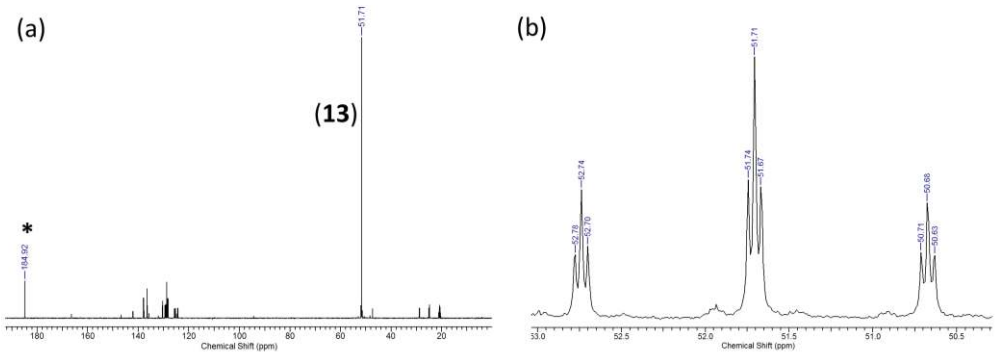

Figure 4: (a) ^{13}C NMR spectrum immediately after the addition of ^{13}CO to a solution of 10 mol% **11** and $PhSiH_3$ highlighting the production of compound **13**. Unreacted ^{13}CO is indicated by *. (b) Expansion of the ^{13}C-labelled methyl resonance at δ 51.7 ppm associated with compound **13** in the corresponding ^{13}C-^{1}H gated NMR spectrum.

We suggest that in both cases the initial step of the catalysis requires the insertion of CO into the M-H bonds of **4** and **11** to form alkaline earth formyl species analogous to those implicated during the formation of compounds **5** and **12**. The absence of any evidence of C_2 or higher homologated products, however, suggests that the reaction between such formyl species and a Si-H bond of phenylsilane occurs more rapidly than any homologation reactivity under one atmosphere of CO for both the magnesium and calcium systems. Although no calcium-derived intermediates could be identified by NMR spectroscopy, some insight into the nature of the CO reduction was provided by a single crystal of a new calcium compound (**15**), which formed at the cessation of a typical catalytic reaction. Although no other data could be obtained for this compound, the results of the X-ray analysis (Figure 5, Table 1) revealed the production of a *C*-silylated calcium methoxide species. Although the presence of a diphenylsilyl substituent indicates that redistribution of the phenylsilane also occurs as a competitive process during the course of the CO reduction,[48] the constitution of compound **15** strongly implicates the

formation of related alkaline earth species as early intermediates *en route* to compounds **13** and **14**

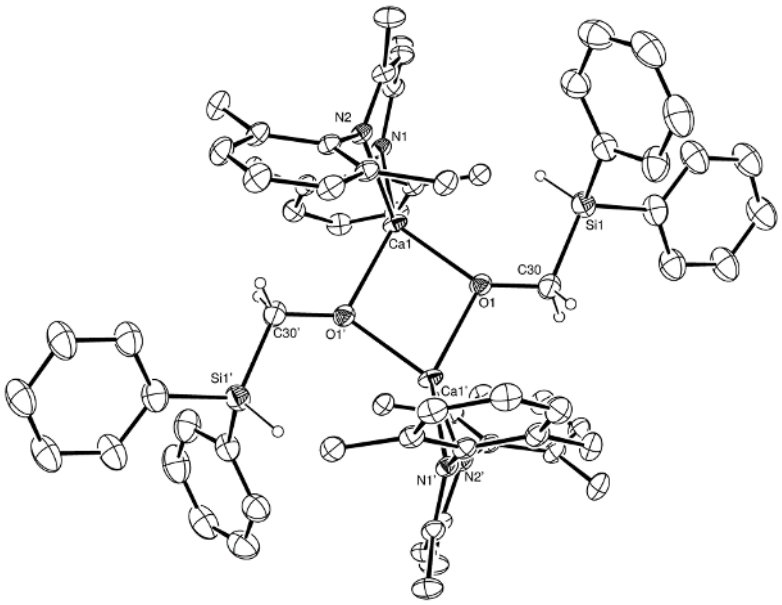

Figure 5: ORTEP representation of compound **15** (25% probability ellipsoids). Hydrogen atoms except those attached to Si1 and C20 and *iso*-propyl methyl carbon atoms are removed for clarity. Selected bond lengths (Å) and angles (°): Ca1–O1 2.2057(15), Ca1–O1′ 2.2507, O1–C30 1.409(3), C30–Si1 1.820(10). O1–Ca1–O1′ 79.90(6), Ca1–O1–Ca1′ 10.10(6), O1–C30–Si1 112.25(16). Atoms with primed labels are related to those in the asymmetric unit by the 2–*x*, 1–*y*, –*z* symmetry operation.

While we were not able to carry out a successful bulk synthesis of further species akin to compound **15**, we suggest the production of such a methoxide species may be rationalized through addition of a Si-H bond to an initially formed carbenic formyl intermediate. The onward trajectory of the catalysis is predicated on a sequence of rapid alkoxide M-O/Si-H and M-H/C-O metathesis events to provide compounds **13** and **14**. The superior ability of the calcium-based reaction to provide **13** is consistent with significantly lower barrier heights for these processes in comparison with those mediated by magnesium. Although the heavier alkaline earth element is apparently unable to effect deoxygenation of the silyl ether, we suggest that this is likely to be a result of the aforementioned solution redistribution at the necessary elevated temperatures, which rapidly depletes the available reactive calcium species. Further insight into these observations was obtained through DFT calculations (B3PW91), which were performed on the complete magnesium-based cycle. The results of this analysis are shown in Figure 6. The production of compound **14** was found to be moderately exothermic ($\Delta H = -79.1$ kcal mol^{-1}) as a result of the thermodynamic stability of

the siloxane by-product. The reaction ensues through the initial generation of a monomeric β-diketiminato κ^2-C,O-formyl complex, which is intercepted by phenylsilane through what may be considered as a facile oxidative addition to the carbenic carbon center. Silane metathesis of the resultant magnesium alkoxide (c.f. compound **15**) provides compound **13** via a moderate barrier of 20.1 kcal mol^{-1} and compound **14** is generated through σ-bond metathesis of the C-O single bond of the methoxysilane with an equivalent of magnesium hydride. This latter reaction represents the rate determining process of the catalysis, requiring the traversal of a barrier of some 33.9 kcal mol^{-1}.

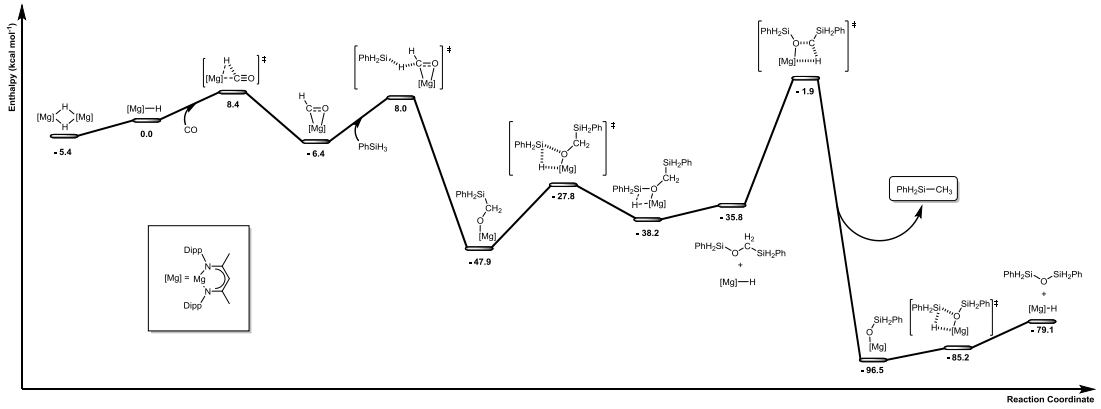

Figure 6: Computed (DFT, B3PW91) energy profile for the silane-based reduction of CO catalyzed by **4**.

Alkaline earth-mediated carbonylation of amines

The observation that the insertion of carbon monoxide into the reactive Ae-H bonds of the β-diketiminato magnesium and calcium hydrides, **4**, **9** and **11**, took place through the initial generation of reactive carbene-like formyl derivatives led us to speculate that further productive reactivity could be developed through the direct carbonylation of Ae-N bonds within magnesium and calcium amides. Although a variety of transition metal-mediated aminocarbonylation reactions have been described,[49] very few lead directly to formamide units, {RNCH(O)},[50] which are important intermediates in the synthesis of a wide variety of fungicide and pharmaceutical compounds, as well as in isocyanate, formamidine, and nitrile formation.[51] Well-defined products from stoichiometric reactions of transition metal amides and CO are similarly uncommon and the sole crystallographically defined example appears to be Bergman's formamide complex, *trans*-[(dmpe)$_2$Fe(H)(NHCHO)] (dmpe = 1,2-bis(dimethylphosphino)ethane), which was prepared by treatment of the parent iron amide *trans*-[(dmpe)$_2$Fe(H)(NH$_2$)] with carbon monoxide.[52, 53] This latter compound was rationalized to have formed via a direct nucleophilic attack of the $[NH_2]^-$ group on the CO carbon. Notably,

this reactivity is also reminiscent of the very limited experimental and theoretical reports that detail the attempted carbonylation of lithium and magnesium amides.[54-59] With these observations in mind we sought to elaborate the carbonylation reactivity of *β*-diketiminato magnesium and calcium amides as a novel route to formamidate derivatives.

In an attempt to synthesise a *β*-diketiminato magnesium derivative of the $[NH_2]^-$ anion, a solution of magnesium hydride complex (**4**) in THF was added to an equimolar solution of ammonia in 1,4-dioxane. This procedure, however, provided an insoluble and intractable colorless powder as the sole reaction product. In contrast, Harder and co-workers have previously reported that the hydrocarbon-soluble calcium amide derivative $[\{HC\{(Me)CNDipp\}_2CaNH_2(NH_3)_2]_2$ may be synthesized by treatment of $[\{HC\{(Me)CNDipp\}_2CaN(SiMe_3)_2(THF)]$ with ammonia gas.[60] Although, in our hands, this reaction resulted in problematic competitive protonation of the *β*-diketiminate ligand, a reaction performed between the calcium hydride (**11**) and an equimolar solution of ammonia in dioxane was found to provide smooth access to the *β*-diketiminato calcium amide complex (**16**, Scheme 5).

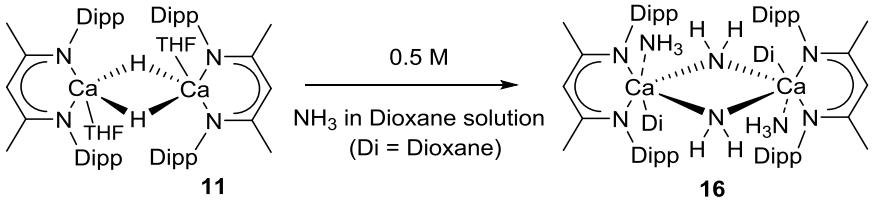

Scheme 5: Synthesis of the calcium amide derivative, **16**.

Storage of the reaction solution at –35 °C overnight resulted in crystallization of large colorless needles suitable for an X-ray diffraction analysis. The results of this experiment are shown in Figure 7 while details of the analysis and selected bond length and angle data are provided in Table 1 the figure caption respectively. The solid state structure of **16** comprises a centrosymmetric dimer, with terminal *β*-diketiminate and symmetrically bridging $[NH_2]^-$ ligands. One additional molecule of ammonia and one dioxane ligand coordinate to each of the distorted octahedral calcium centers. The structure of compound **16** is otherwise strongly reminiscent of the bis-ammonia coordinated calcium amide $[HC\{(Me)CNDipp\}_2CaNH_2(NH_3)]_2$ reported by Ruspic and Harder obviating further comment.[60] Although exposure of **16** to a dynamic vacuum at room temperature resulted in decomplexation of the NH_3 ligands, the dioxane donors remained coordinated, even at elevated temperatures (ca. ~80 °C).

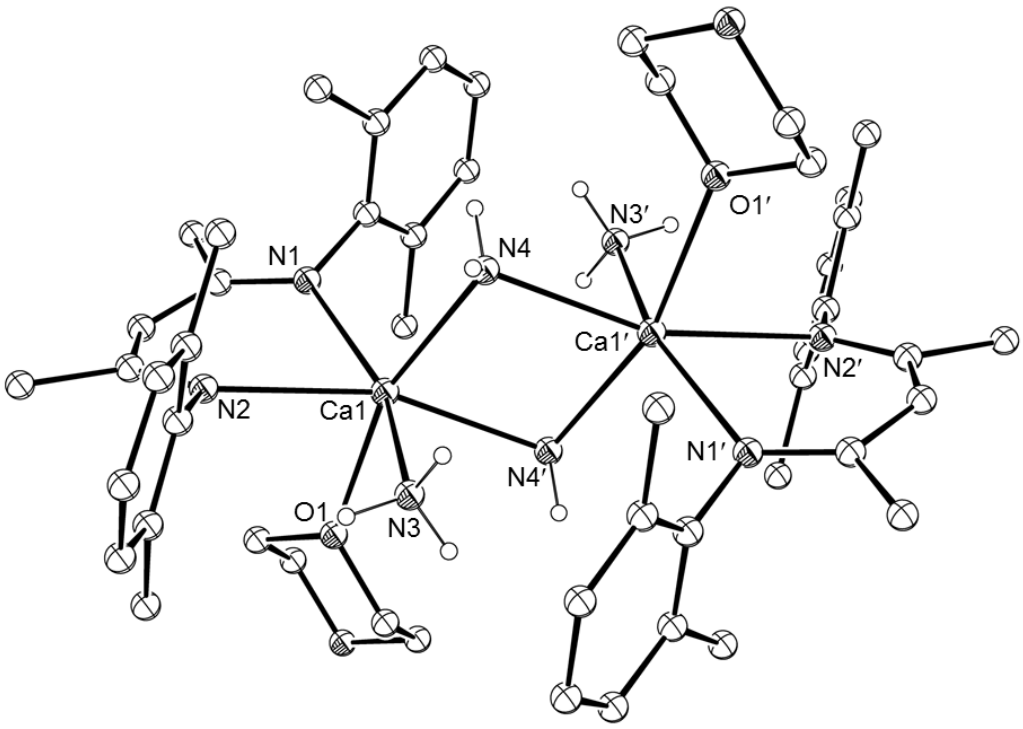

Figure 7: ORTEP representation of **16** (25% probability ellipsoids). All carbon-bound hydrogen atoms and *iso*-propyl methyl carbon atoms are removed for clarity. Selected bond lengths (Å) and bond angles (°): Ca1–O1 2.5247(12), Ca1–N1 2.5030(12), Ca–N2 2.5264(12), Ca1–N3 2.5551(14), Ca1–N4 2.4431(12), O1–Ca1–N2 84.15(4), O1–Ca1–N3 94.27(5), N1–Ca1–O1 92.06(4), N4–Ca1–O1 84.15(4), N1–Ca1–N2 75.69(4), N1–Ca1–N3 157.30(4), N2–Ca1–N3 83.30(4), N4′–Ca1–N1 97.84(4), N4–Ca1–N1 119.81(4), N4′–Ca1–N2 111.66(4), N4–Ca1–N2 160.89(4), N4′–Ca1–N3 81.87(5), N4–Ca1–N3 82.56(5), N4′–Ca1–N4 78.92(5), Ca1–N4–Ca1′ 101.08(5). Atoms with primed labels are related to those in the asymmetric unit by the 1–*x*, 2–*y*, –*z* symmetry operation.

A sample of compound **16** in d_8-toluene was exposed to one atmosphere of ^{13}CO. Interrogation of the resultant ^{1}H and ^{13}C NMR spectra revealed complete consumption of the calcium starting material at the first point of analysis. The presence of a new singlet resonance at δ 174.3 ppm in the ^{13}C NMR spectrum, confirmed that no carbon-carbon coupling had occurred. In the ^{13}C-^{1}H gated spectrum this resonance was observed to split into a doublet of doublets, ($^{1}J_{CH}$ = 183.1, $^{2}J_{CH}$ = 2.9 Hz) consistent with the formation of a new ^{13}C-H bond, adjacent to a further single proton with a *β*-disposition with respect to the carbon nucleus. A subsequent HSQC experiment identified a corresponding doublet of doublets at δ 6.58 ppm ($^{1}J_{HC}$ = 183.1, $^{3}J_{HH}$ = 6.1 Hz) in the ^{1}H NMR spectrum. This spectrum also comprised a highly shielded and broadened singlet resonance at δ −2.04 ppm which corresponded to a single proton by relative integration and provided no carbon correlation in the corresponding HSQC experiment. This

signal was, thus, assigned as arising from the N-H unit of a new calcium formamidate complex, compound **17** (Scheme 6).

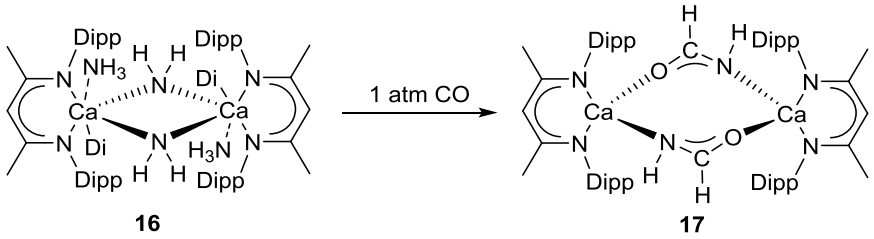

Scheme 6: Synthesis of the calcium formamidate complex, compound **17**.

A saturated THF/hexane solution of **17**, which was allowed to slowly evaporate for 3 days at room temperature, afforded crystalline colorless blocks suitable for a single crystal X-ray diffraction experiment. The results of this experiment are illustrated in Figure 8 while details of the analysis and selected bond length and angle data are provided in Table 1 and the figure caption respectively. The solid state structure of **17** comprises a dimeric *β*-diketiminato calcium complex with asymmetrically bridging formamidate ligands. The {O1-C30-N3}-containing anion bridges symmetrically via μ_2–interactions between O1 and N3 and both Ca1 and Ca2, whereas the {O2-C31-N4}-containing ligand adopts an approximately orthogonal disposition to the first formamidate and coordinates via N4-Ca2 and μ_2-O2 interactions. Both calcium centers, Ca1 and Ca2, thus, display a distorted octahedral geometry with the final coordination site on Ca1 filled by a THF ligand. The solution structure of **17** at room temperature did not allow for differentiation between the two formamidate moieties by ^{1}H and ^{13}C NMR spectroscopy even at reduced temperature down to the lower limit of –93 °C, indicating that exchange between the two formamidate ligand bonding modes is facile and occurs faster than the NMR timescale.

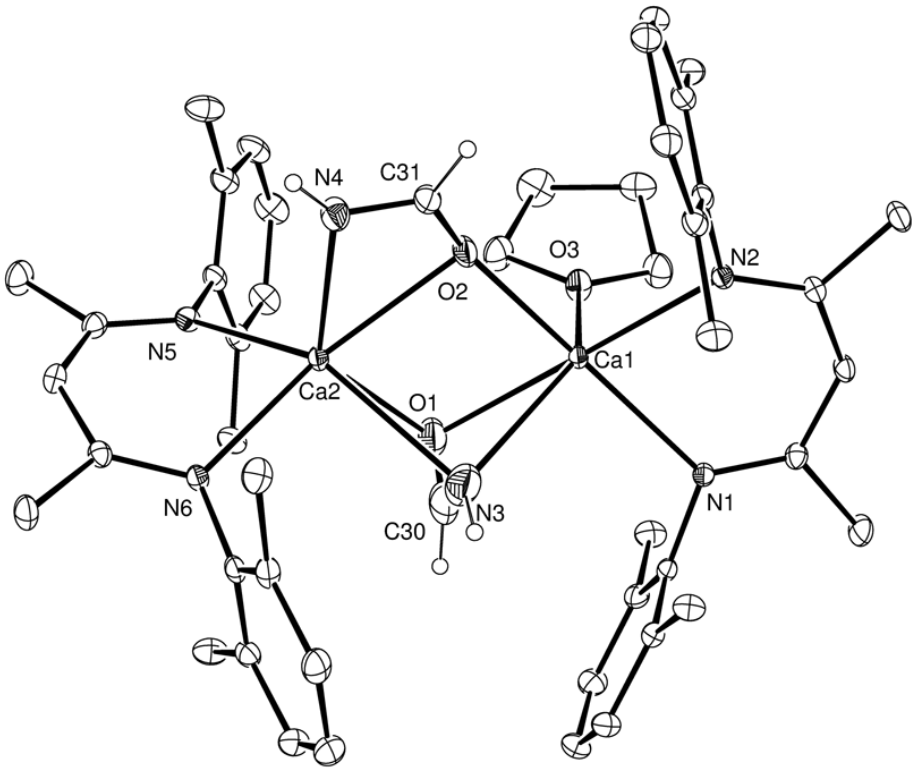

Figure 8: ORTEP representation of **17** (25% probability ellipsoids). Hydrogen atoms, except those attached to N3, N4, C30 and C31, and *iso*-propyl methyl carbon atoms have been removed for clarity. Selected bond lengths (Å) and bond angles (°): Ca1–O1 2.476(2), Ca1–O2 2.2602(16), Ca1–O3 2.3538(15), Ca1–N1 2.4053(16), Ca1–N2 2.4061(16), Ca1–N3 2.575(3), Ca2–O1 2.443(2), Ca2–O2 2.4473(15), Ca2–N3 2.616(3), Ca2–N4 2.4468(19), Ca2–N5 2.3649(16), Ca2–N6 2.3600(16), O1–C30 1.191(5), O2–C31 1.284(3), N3–C30 1.302(5), N4–C31 1.270(3), O1–Ca1–N3 50.18(10), O2–Ca1–O1 81.99(6), O2–Ca1–O3 94.57(7), O2–Ca1–N1 166.73(7), O2–Ca1–N2 95.80(6), O2–Ca1–N3 80.60(8), O3–Ca1–N3 80.60(8), O3–Ca1–O1 83.82(8), O3–Ca1–N1 98.13(6), O3–Ca1–N2 99.65(6), O3–Ca1–N3 134.00(9), N1–Ca1–O1 103.15, N1–Ca1–N2 78.32(5), N1–Ca1–N3 93.23(7), N2–Ca1–O1 176.05(7), N2–Ca1–N3 126.32(9), O1–Ca2–O2 79.00(6), O1–Ca2–N3 49.99(10), O1–Ca2–N4 132.59(7), O2–Ca2–N3 76.47(8), N4–Ca2–O2 53.84(6), N4–Ca2–N3 107.28(9), N5–Ca2–O1 103.66(8), N5–Ca2–O2 123.06(7), N5–Ca2–N3 146.75(9), N5–Ca2–N4 105.89(7), N6–Ca2–O1 108.91(7), N6–Ca2–O2 154.60(7), N6–Ca2–N3 90.14 (7), N6–Ca2–N4 112.31(6), N6–Ca2–N5 79.48(6).

Encouraged by the isolation of the parent formamidate derivative **17** this reactivity was extended to the carbonylation of *β*-diketiminato magnesium and calcium aryl and alkyl amides, ([(HC{(Me)CNDipp}$_2$AeNHR)], Ae = Mg or Ca and R = aryl or alkyl). Although we have previously described the isolation of a variety of amide and anilide derivatives of both

alkaline earth metals supported by the identical β-diketiminate ligand,[62, 63] these reactions were most conveniently performed through the *in situ* protonolysis of either compound **4** or **11** by a stoichiometric equivalent of the appropriate amine or aniline in d_8-toluene. The resultant solutions were then degassed and exposed to 1 atmosphere of ^{13}CO at room temperature.

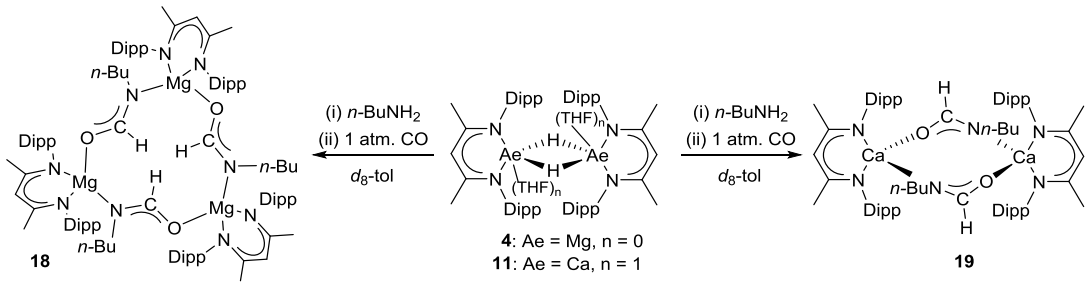

Scheme 7: Synthesis of compounds **18** (Ae = Mg) and **19** (Ae = Ca) through the reaction of i*n situ*-generated β-diketiminato magnesium and calcium *n*-butyl amide complexes and 1 atm. ^{13}CO.

An initial reaction was performed between compound **4** and *n*-$BuNH_2$ in d_8-toluene. Although interrogation of this reaction by ^1H and ^{13}C NMR spectroscopy immediately after addition of ^{13}CO indicated that no reaction had occurred, reassessment after 12 hours at room temperature demonstrated ca. 30% conversion to a new compound (**18**), thought to be the alkyl formamidate which was identified through the appearance of two new highly deshielded doublet signals at δ 7.87 ppm and 6.88 ppm ($^1J_{CH}$ = 177.4 Hz and $^1J_{CH}$ = 182.9 Hz) in a two to one ratio in the ^1H NMR spectrum. Elevation of the reaction temperature to 60 °C for 12 hours provided complete conversion to **18**, as identified by the emergence of a two singlet resonances at δ 171.9 ppm and δ 165.0 ppm in the $^{13}C\{H^1\}$ NMR spectrum. The signal at δ 171.9 ppm was observed to split into a sharp doublet of triplets ($^1J_{CH}$ = 177.4, $^3J_{CH}$ = 9.9 Hz) while the signal at δ 165.0 ppm split into a broad doublet ($^1J_{CH}$ = 182.9 Hz) in the ^1H–^{13}C gated spectrum, indicating CO insertion had occurred with a 1,2–hydrogen shift from the nitrogen to the carbon to provide an alkyl formamidate product in two different environments (*vide infra*). In contrast to this relatively slow conversion, monitoring by ^1H NMR spectroscopy of an analogous reaction performed with the calcium hydride **11** indicated complete conversion to a single new compound, **19**, at the first point of analysis after the addition of ^{13}CO. Examination of the ^{13}C NMR spectrum revealed the appearance of a new resonance at δ 168.8 ppm that in the ^{13}C-^1H gated spectrum split into a doublet of triplets ($^1J_{CH}$ = 180.5, $^3J_{CH}$ = 8.1 Hz) confirming the formation of a new C-H bond. A corresponding doublet observed at δ 8.06 ppm ($^1J_{HC}$ = 180.5 Hz) in the ^1H NMR spectrum with a relative integral of 1H was clearly indicative of the formation of a calcium *N*-*n*-butyl formamidate derivative (Scheme 7).

Storage of the reaction solutions used in the synthesis of compounds **18** and **19** at –35 °C yielded large colorless block crystals suitable for X-ray diffraction analysis. The solid state structure of **18**, revealed a trimeric magnesium structure (Figure 9), in which three *N*-*n*-butyl formamidate moieties and three magnesium centers comprise a near planar, twelve membered heterocycle. Each formamidate ligand bonds in a κ^1-fashion from the oxygen to one magnesium center and κ^1- from its respective nitrogen to a second magnesium center to make up one third of the trimeric structure. Each magnesium is also bound to a bidentate *β*-diketiminate ligand, which is approximately orthogonal to the plane defined by the twelve-membered heterocycle, to complete a distorted tetrahedral coordination geometry. The solid state structure of **18** also demonstrates that the hydrogen atoms attached the C59 and C64 lie on one side the heterocyclic plane, whilst the hydrogen attached to C98 lies on the opposite side of the plane. The different formamidate environments evidenced in the solution structure of **18** are, thus, tentatively assigned to these spatially inequivalent hydrogen atoms. Variable temperature experiments provided no simplification of the ^{1}H NMR spectra at either reduced or elevated temperatures, indicating that the formamidate methine resonances continue to be conformationally differentiated on the NMR timescale.

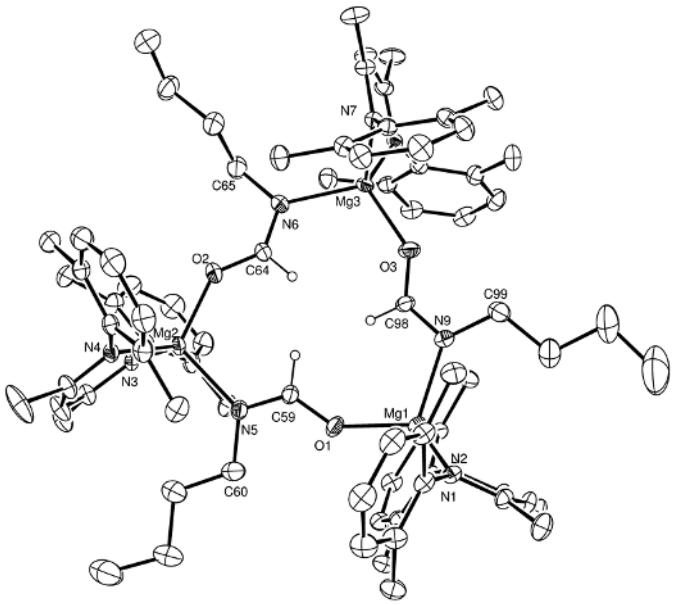

Figure 9: ORTEP representation of **18** (25% probability ellipsoids). Hydrogen atoms, except those attached to C59, C64 and C98, and *iso*-propyl methyl carbon atoms have been removed for clarity. Selected bond lengths (Å) and bond angles (°): Mg1–O1 1.9088(18), Mg1–N1 2.0339(18), Mg1–N2 2.0436(17), Mg1–N9 2.099(2), Mg2–O2 1.9272(18), Mg2–N3 2.0389(19), Mg2–N4 2.0493(19), Mg2–N5 2.110(2), O1–C59 1.281(3), O2–C64 1.266(3), N5–C59 1.291(3), N6–C64 1.277(3). O1–Mg1–N1 111.23(8), O1–Mg1–N2 114.53(8), O1–Mg1–N2 95.13(7), N1–Mg1–N9 116.33(8), N2–Mg1–N9 109.82(8), O2–Mg2–N3 108.69(8), O2–Mg2–N4 118.01(8), O2–Mg2–N5 111.50(8), N3–Mg2–N4 95.08(8), N3–Mg–N5

113.875(8), N4–Mg2–N5 108.95(8), O1–C59–N5 126.7(2), O2–C64–N6 130.1(2), O3–C98–N9 126.8(2).

The X-ray diffraction analysis of compound **19** revealed a contrasting dimeric complex (Figure 10). The bidentate *β*-diketiminate ligands coordinate to the six-coordinate calcium centers in a manner reminiscent of **17**, with symmetrically bridging *n*-butyl formamidate ligands, which adopt a mutual coplanar orientation. The {O1-C59-N5}-containing formamidate ligand binds in a κ^2-fashion to Ca1 with a bridging interaction to Ca2 through O1 while the formamidate displays an identical bonding mode but via chelation of Ca2 through O2 and N6 and coordination to Ca1 through the μ_2-O2 center.

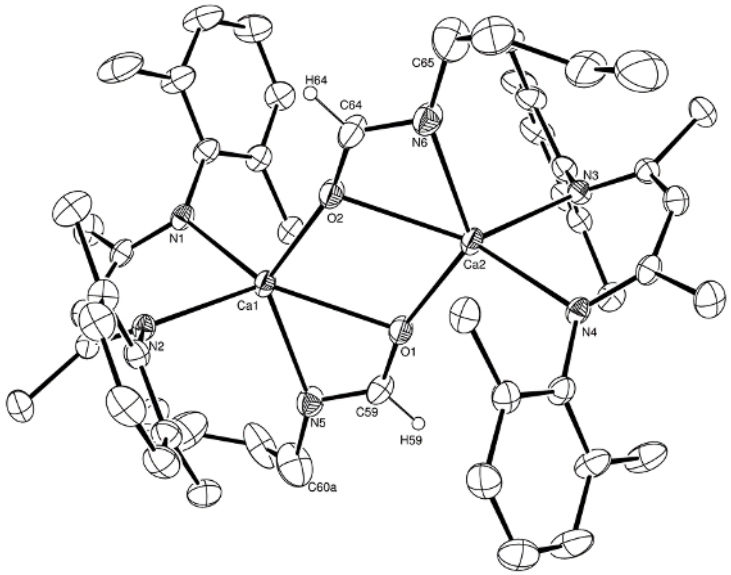

Figure 10: ORTEP representation of **19** (25% probability ellipsoids). Hydrogen atoms, except those attached to C59 and C64, and *iso*-propyl methyl carbon atoms have been removed for clarity. Selected bond lengths (Å) and bond angles (°): Ca1–O1 2.4470(17), Ca1–O2 2.2387(19, Ca1–N1 2.3284(19), Ca1–N2 2.3333(19), Ca1–N5 2.466(2), Ca1–C59 2.811(3), Ca2–O1 2.2351(19), Ca2–O2 2.4501(17), Ca2–N3 2.3295(19), Ca2–N4 2.3235(18), Ca2–N6 2.450(2), Ca2–C64 2.802(3), N5–C59 1.275(4), N6–C64 1.272(4), O1–C59 1.297(3), O2–C64 1.290(3). O1–Ca1–N5 54.41(7), O2–Ca1–N1 108.42(7), O2–Ca1–N2 112.74(7), N1–Ca1–N2 82.84(7), O2–Ca1–N5 130.33(7), O1–Ca2–N3 114.56(7), O1–Ca2–N4 108.62(7), N6–Ca2–O2 54.39(7), N4–Ca2–N3 81.05(7), N5–C59–O1 121.7(2), N6–C64–O2 121.9(3).

Encouraged by these results, the scope of this amide carbonylation reaction was extended to the range of *in situ* generated alkyl and aryl amides summarised in Scheme 8. Exposure of the *in situ* generated *β*-diketiminato magnesium and calcium amide complexes to 1 atmosphere of ^{13}CO led to the facile formation of the corresponding alkyl and aryl formamidates,

compounds **20** - **24**. In the case of the magnesium complexes, increasing amine substituent steric demands required significantly longer reaction times for reactions performed at 60 °C (**20**: 48 h; **21**: 72 h), while complete conversion to compound **22** necessitated heating of the reaction to 100 °C for 72 hours. Although a further reaction of CO with the calcium anilide derived from the sterically demanding $DippNH_2$ to yield compound **25** *vide infra*),[64] required heating to 60 °C, the formation of the *N*-alkyl formamidate calcium compounds **23** and **24** was complete within 1 hour at room temperature.

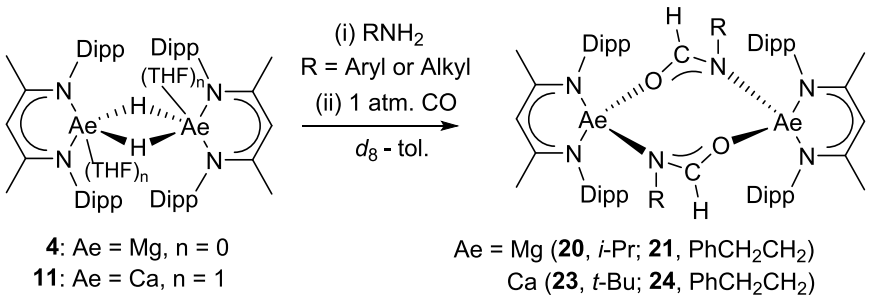

Scheme 8: Synthesis of compounds **20**, **21**, **23** and **24**.

The structures of the new compounds **20**, **21**, **23** and **24** were confirmed by single crystal X-ray diffraction analysis. The results of the analyses of the magnesium *N*-alkyl formamidates, **20** and **21**, are shown in Figure 11, while details of the X-ray experiments and selected bond length and angle data are provided in Table 2 and the figure caption respectively. In contrast to the trimeric structure of compound **18** and the monomeric constitution of compound **22**, which has been previously synthesized through reaction of compound **4** and DippNCO,[65] both **20** and **21** are dimeric in the solid state. Although the symmetrical bridging mode of the *N*-*iso*-propyl formamidate ligands between the distorted trigonal bipyramidal magnesium centers in compound **20** is reminiscent of that observed for the calcium complex **19**, the subtle influence of varying steric demands on the structures of these heteroleptic magnesium formamidates was apparent in the structure of compound **21**. In this case only the {O1-C30-N3}-containing *N*-ethylphenyl-substituted formamidate anion adopts a Mg1-chelated orientation in which O1 bridges in a μ_2-fashion between Mg1 and Mg2. Presumably for steric reasons, Mg2 in the structure of **21** is four- rather than five-coordinate and the second {N4-C39-O2}-containing formamidate adopts an alternative κ^1-Mg1-O2/κ^1-Mg2-N4 bridging mode.

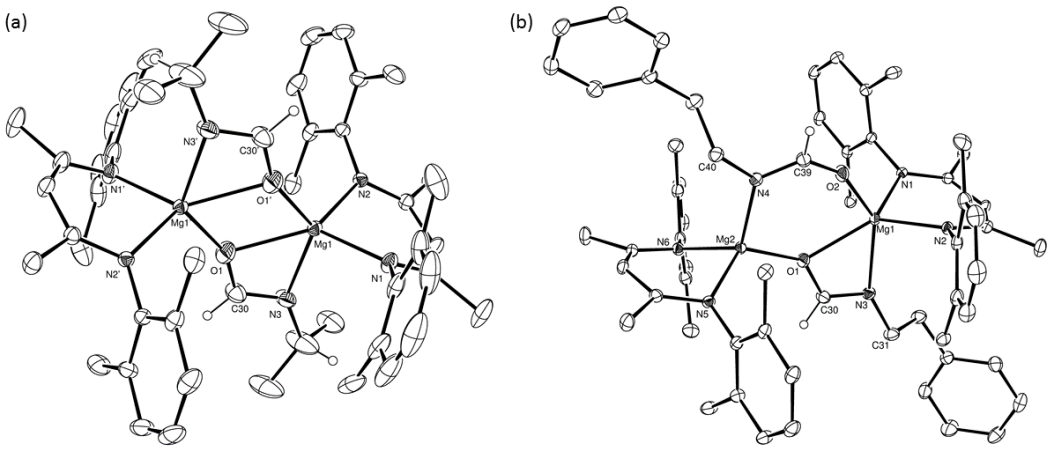

Figure 11: ORTEP representations of (a) **20** and (b) **21** (25% probability ellipsoids). Hydrogen atoms except those attached to the C30 and C39 and *iso*-propyl methyl carbon atoms are removed for clarity. Selected bond lengths (Å) and bond angles (°): (**20**) Mg1–N2 2.0810(15), Mg1–N1 2.0751(17), Mg1–O1′ 1.9901(17), Mg1–O1 2.1789(18), Mg1–N3 2.240(2), N3–C30 1.259(3), O1–C30 1.299(3). N2–Mg1–O1 129.64(7), N2–Mg1–N3 103.45(7), N1–Mg1–N2 92.61(6), N1–Mg1–O1 135.13(7), N1–Mg1–N3 102.24(8), O1–Mg1–N3 58.69(7), N3–C30–O1 115.8(2); (**21**) Mg1–O1 2.1727(14), Mg1–O2 1.9612(14), Mg1–N1 2.0711(15), Mg1–N2 2.0700(15), Mg1–N3 2.2698(16), Mg2–O1 1.9409(13), Mg2–N4 2.0760(16), Mg2–N5 2.0604(15), Mg1–N6 2.0476(15), O1–C30 1.310(2), O2–C39 1.255(2), N3–C30 1.267(2), N4–C39 1.297(2). O1–Mg1–N3 59.51(5), O2–Mg1–O1 86.23(5), O2–Mg1–N1 106.65(6), O2–Mg1–N2 99.87(6), O2–Mg1–N2 144.22(6), N2–Mg1–N1 92.65, O1–Mg2–N4 104.15(6), O1–Mg2–N5 122.66(6), O1–Mg2–N6 112.30(6), N5–Mg2–N4 106.15(6), N6–Mg2–N4 118.40(6), N3–C30–O1 117.78(16), O2–C39–N4 126.59(18). Atoms with primed labels in **20** are related to those in the asymmetric unit by the 1–*x*, 2–*y*, –*z* symmetry operation.

It was possible to discriminate between the individual bonding modes of the two *N*-phenyl ethyl formamidate ligands of compound **21** by NMR spectroscopy at 298 K. One formamidate methine center was manifested as a heavily deshielded signal at δ 173.0 ppm, ($^1J_{CH}$ = 176.1, $^3J_{CH}$ = 9.5 Hz) in the ^{1}H-^{13}C gated NMR spectrum, with a corresponding resonance at δ 7.84 ppm, (d, $^1J_{HC}$ = 176.1 Hz) in the ^{1}H NMR spectrum. The second ligand environment was apparent as a further pair of similarly correlated signals, which were observed in the ^{1}H-^{13}C gated (δ 168.0 ppm, $^1J_{CH}$ = 180.5, $^3J_{CH}$ = 8.6 Hz) and ^{1}H NMR spectra (δ 7.81 ppm, 1H, d, $^1J_{HC}$ = 180.5 Hz).

Whereas the structures of the magnesium derivatives (**19** – **21**) display a distinct dependence on the steric demands of the aliphatic *N*-amine employed, the solid state structures

of the calcium compounds **23** and **24** (Figure 12, Table 2) bear close comparison to the dimeric *N*-butyl formamidate derivative **19**, rendering further comment unnecessary.

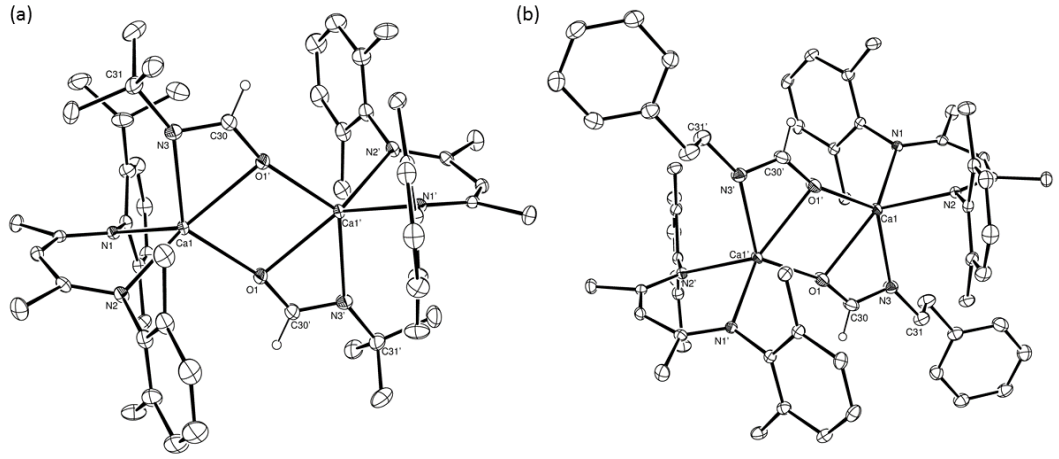

Figure 12: ORTEP representations of (a) **23** and (b) **24** (25% probability ellipsoids). Hydrogen atoms except those attached to C30 and C30′ and *iso*-propyl methyl carbon atoms are removed for clarity. Selected bond lengths (Å) and bond angles (°): (**23**) Ca1–O1 2.2549(12), Ca1–O1′ 2.4211(13), Ca1–N1 2.3392(13), Ca1–N2 2.3263(14), Ca1–N3 2.4472(15), N3–C30 1.288(3), O1–C30′ 1.303(2). O1–Ca1–O1′ 76.26(5), O1–Ca1–N1 110.49(5), O1–Ca1–N2 107.18(5), O1′–Ca1–N3 55.20(5), O1–Ca1–N3 131.21(5), N2–Ca1–N1 81.99(5), N1–Ca1–N3 107.33(5), N2–Ca1–N3 107.59(5), N3–C30–O1′ 121.08(17); (**25**) Ca1–O1′ 2.2528(14), Ca1–O1 2.4198(13), Ca1–N1 2.3293(14), Ca1–N2 2.3339(14), Ca1–N3 2.4834(16), N3–C30 1.274(3), O1–C30 1.293(2). O1–Ca1–O1′ 76.01(5), O1–Ca1–N3 54.67(5), N1–Ca1–O1 138.11(5), N1–Ca1–N2 83.50(5), N1–Ca1–N3 108.70(5), N2–Ca1–N3 102.59(5), N3–C30–O1 121.56(18). Atoms with primed labels are related to those in the asymmetric unit by the ½–*x*, ½–*y*, –*z* and –*x*, –*y*, 2–*z* symmetry operations in **23** and **24**, respectively.

Synthesis of the more sterically congested calcium *N*-Dipp formamidate, [HC{(Me)CN(Dipp)}$_2$Ca{OC(H)N(Dipp)}], (**25**) required heating (60 °C) to induce insertion of ^{13}CO into the Ca-N(H)Dipp bond. Removal of volatiles and dissolution in hexane gave colorless blocks at −35 °C, which were suitable for an X-ray diffraction analysis. The solid state structure of compound **25** did not display a monomeric structure analogous to that previously observed for **22**. Rather, compound **25** crystallized as a heteroleptic bimetallic species comprising two dissimilar calcium centers (Figure 13), which evidently forms as a consequence of the greater tendency of the larger and more labile alkaline earth center to undergo Schlenk-like solution redistribution.[64] A solitary bidentate *β*-diketiminate ligand is

bound to the six-coordinate Ca1 center and three *N*-Dipp formamidate ligands coordinate in a μ_2-fashion between both calcium centers via each of the O1, O2 and O3 formamidate oxygen atoms. A molecule of THF occupies the final Ca1 coordination site, while the coordination sphere of the second calcium center, Ca2, is provided by three bidentate *N*-Dipp formamidate ligands, which bind in a κ^2-fashio nfrom each of the oxygen and nitrogen donors. A second terminal THF molecule provides the final contact to Ca2 to complete a distorted pentagonal bipyramidal coordination geometry.

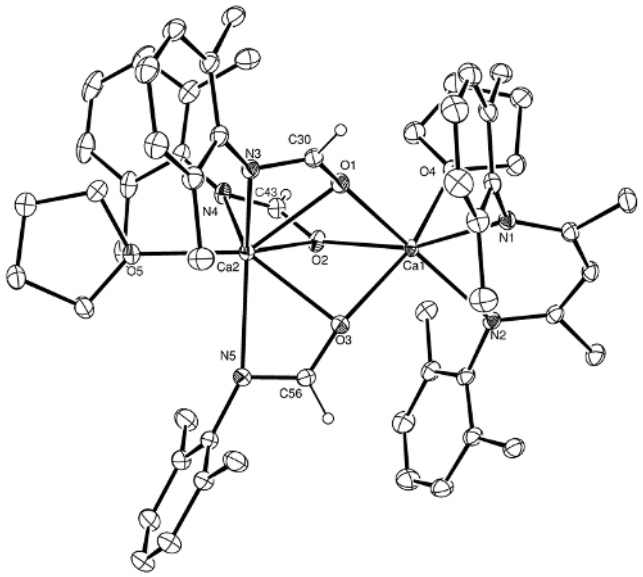

Figure 13: ORTEP representation of **25** (25% probability ellipsoids). Hydrogen atoms except those attached to C30, C43 and C56 and *iso*-propyl carbon atoms are removed for clarity. Selected bond lengths (Å) and bond angles (°): Ca1–O1 2.3338(13), Ca1–O2 2.3809(14) Ca1–O3 2.3330(14), Ca2–O1 2.4183(14), Ca2–O2 2.4953(14), Ca2–O3 2.4212(14), Ca1–N1 2.4300(16), Ca1–N2 2.4188(15), Ca2–N3 2.5113(16), Ca2–N4 2.4995(17), Ca2–N5 2.5572(17), O1–C30 1.288(2), O2–C43 1.278(2), O3–C56 1.284(2), N3–C30 1.291(2), N4–C43 1.294(3), N5–C56 1.298(3). O1–Ca1–O2 75.01(5), O1–Ca1–O4 101.22(5), O1–Ca1–N1 92.49(5), O1–Ca1–N2 165.92(5), O2–Ca1–N1 162.71(5), O2–Ca1–N2 116.84(5), O3–Ca1–N1 114.04(5), O3–Ca1–N2 98.69(5), O1–C30–N3 120.97(18), O2–C43–N4 122.01(18), O3–C56–N5 121.91(18), O1–Ca2–O2 71.48(5), O1–Ca2–O3 73.15(5), O1–Ca2–N3 54.14(5), O2–Ca2–N4 53.54(5),O3–Ca2–N5 53.84(5).

Mechanistic Considerations

Based on these observations and the pathway delineated for the formation of compounds **5**, **10** and **12** (Scheme 1, Figure 3) a likely initial step in the amide carbonylation reaction pathway was rationalized to involve CO insertion into the M-N bond of the alkaline earth amide to yield an intermediate carboxamide complex. In a manner reminscent of the

production of compounds **7** and **5** in Scheme 1, the ultimate *β*-diketiminato alkaline earth formamidate products may then be formed through a facile isomerization process involving a 1,2-nitrogen-to-carbon transfer of the hydrogen atom of the primary amide (Scheme 9).

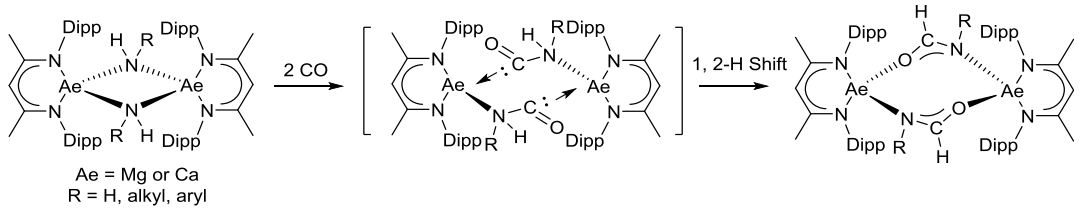

Scheme 9: Proposed reaction pathway for the formation of compounds **17** – **25** through the direct carbonylation of alkaline earth primary amides.

Although no intermediate species during the synthesis of compounds **17**- **25** could either be isolated or identified by NMR spectroscopy, a related reaction between compound **4** and *N*-methylaniline, performed at room temperature and subsequently placed under one atmosphere of ^{13}CO, provided strong corroberative evidence for the mechanistic pathway shown in Scheme 9. Although no evidence of ^{1}H-^{13}C coupling could be observed in the resultant ^{1}H NMR spectrum, the ^{13}C NMR spectrum comprised a diagnostic and highly deshielded resonance at δ 230.0 ppm associated with a new carboxamide magnesium derivative (**26**). Crystallization from the reaction solution provided crystals of compound **26** suitable for an X-ray diffraction analysis. The results of this analysis (Figure 14, Table 2) demonstrated that the structure of **26** is a centrosymmetric dimer and confirmed its consitution as an alkoxoamidocarbene derivative in which both of the carbamoyl ligands bridge the magnesium centers. The carbonyl (O1-C30) bond length of 1.252(2) Å is suggestive of the maintainance of significant double bond character, while the Mg1-C30 bond length [2.2051(19) Å] lies within the range (2.194 – 2.279 Å) of values reported for Mg-C bonds in a variety of magnesium adducts of *N*-heterocyclic carbenes.[66-68]

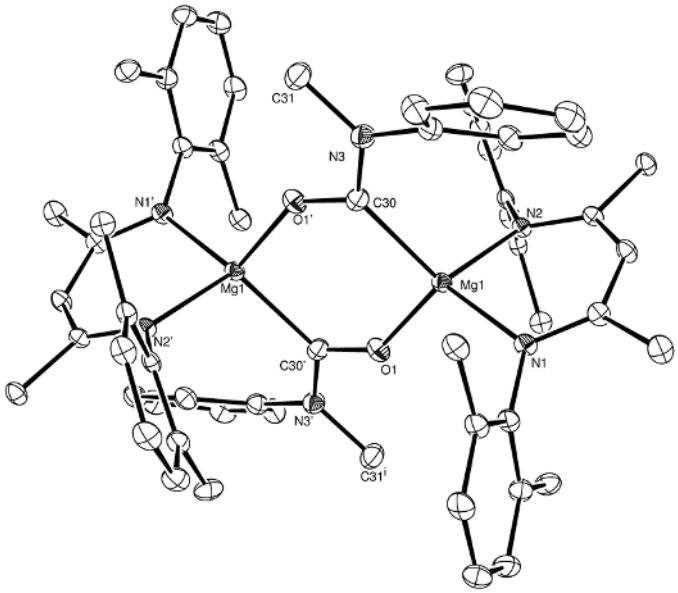

Figure 14: ORTEP representation of **26** (25% probability ellipsoids). Hydrogen atoms and *iso*-propyl methyl carbon atoms are removed for clarity. Selected bond lengths (Å) and bond angles (°): Mg1–N1 2.0580(15), Mg1–N2 2.0774(14), Mg1–O1 1.9239(14), Mg1–C30 2.2051(19), O1–C30′ 1.252(2), N3–C30 1.382(3), N3–C32 1.425(2), N3–C31 1.464(3). N2–Mg1–C30 112.09(6), O1–Mg1–N2 113.23(6), O1–Mg1–N1 111.00(6), O1–Mg–C30 104.00(7), N1–Mg1–N2 93.79(6), N1–Mg1-C30 122.91(7), C30′–O1–Mg1 140.15(13), C30–N3–C32 122.13(16), C30–N3–C31 120.88(16), C32–N3–C31 116.85(16), O1′–C30–Mg1 111.15(13), O1′–C30–N3 114.15(16), N3–C30–Mg1 133.81(13). Atoms with primed labels are related to those in the asymmetric unit by the 1–*x*, 1–*y*, –*z* symmetry operation.

The mechanism of the amine carbonylation reaction was further investigated through DFT calculations (B3PW91), which were performed on the carbonylation of a calcium anilide generated through the reaction of compound **11** and $PhNH_2$. Initial calculations demonstrated the generation of the dimeric *β*–diketiminato calcium anilide to be mildly exothermic, (ΔH = –4.9 kcal mol^{-1}). The disruption of the resultant dimeric calcium anilide complex through the formal insertion of CO into the Ca–N bond, requires the traversal of a significant barrier of some 25.5 kcal mol^{-1} (Figure 15) while CO reduction is computed to be sequential rather than simultaneous. Although the resultant carboxanilide intermediate, which is analogous to the isolable magnesium derivative **26**, exists as a local minimum and its rearrangement to the formamidate species entails two accessible kinetic barriers (23.0 and 22.1 kcal mol^{-1}), the formation of the ultimate calcium *N*-phenyl formamidate is highly exothermic (ΔH = –67.7 kcal mol^{-1}) with respect to the starting materials.

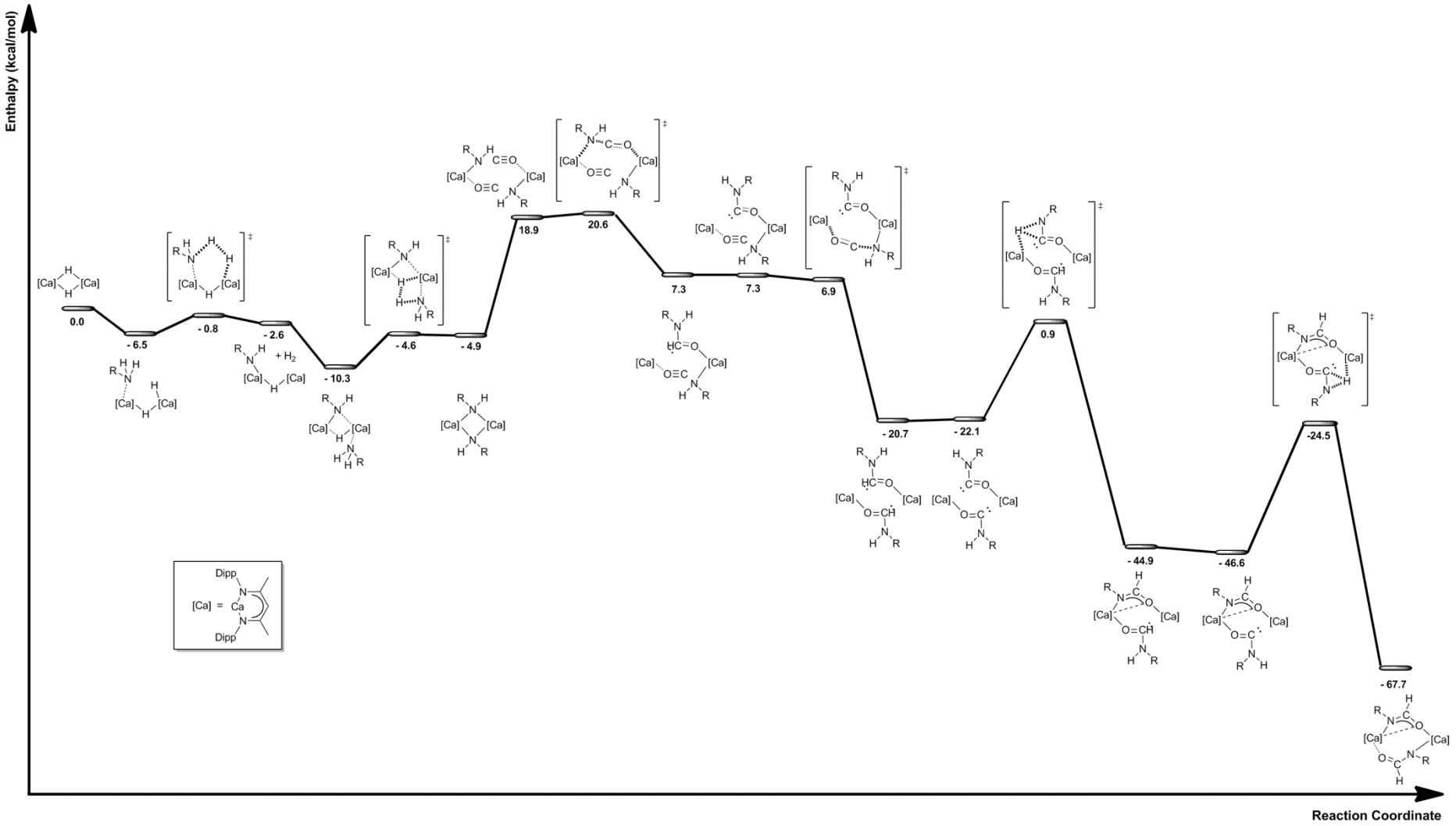

Figure 15: Computed (DFT, B3PW91) energy profile for the initial protolytic reaction between aniline and **11** and the subsequent mechanism of carbonylation.

Calcium Formamidate Hydrodeoxygenation

We have recently reported that magnesium formamidate derivatives directly analogous to compounds **18** and **20** - **22** may also be formed by the direct reaction of an organic isocyanate with compound **4**.[65] Furthermore, these species are readily deoxygenated through reaction with pinacol borane (HBpin) to provide access to borylated methyl amine derivatives under magnesium-catalyzed conditions. Mechanistic and computational studies of this reactivity delineated a mechanism dependent on a sequence of isocyanate hydroboration and C-O insertion steps, which occurs through the intermediacy of a variety of borylated amidate and hemiaminal intermediates (Scheme 10(a)). The C-O cleavage reaction and the ultimate generation of the methyl amine product was deduced to occur with production of a magnesium boryloxide species, $[\{HC(Me)NDipp\}_2MgOBpin]_2$, while the thermodynamic viability of the catalytic reaction is ensured through the consumption of this species by reaction with a further equivalent of HBpin.

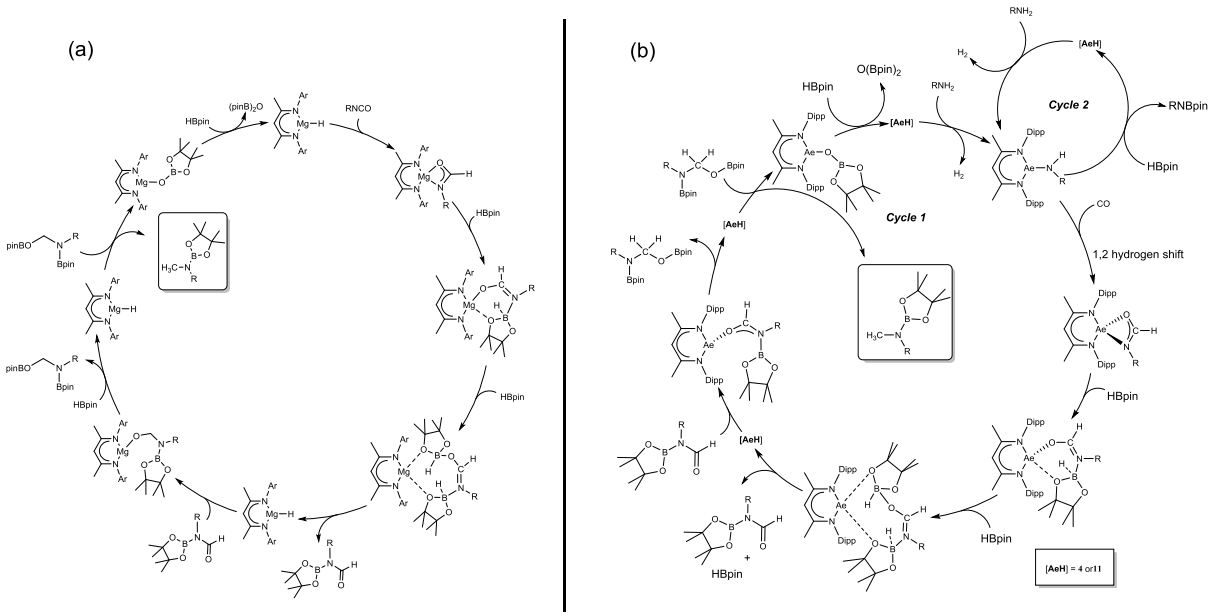

Scheme 10: (a) proposed mechanism for the magnesium-catalyzed hydrodeoxygenation of organic isocyanates; (b) proposed catalytic cycle for the hydrodeoxygenation of CO sequestered formamidates by **4** or **11**.

On this basis, it was postulated that the addition of three equivalents of HBpin to compound **17**, prepared from ^{13}CO, would result in similar formamidate deoxygenation to yield the bis(borylated) *N*–methyl amine, $(pinB)_2N^{13}CH_3$ and a calcium boryloxide analogous to the magnesium boryloxide identified as a key intermediate during our study of isocyanate hydroboration (Scheme 10(a)). Although the fate of the calcium β-diketiminate complex could not be unambiguously identified, immediate interrogation of this reaction by NMR spectroscopy after the addition of HBpin verified the formation of $(pinB)_2N^{13}CH_3$. The ^{13}C NMR spectrum comprised a major resonance at δ 30.9 ppm, which was observed to split into

a binomial quartet ($^1J_{CH}$ = 136.4 Hz) in the corresponding ^1H–^{13}C gated spectrum. Further evidence for the formation of the borylated *N*–methyl amine product was established through the appearance of a doublet resonance at δ 2.05 ppm in the ^1H NMR spectrum, which was shown to be correlated with the resonance at δ 30.9 ppm in the ^{13}C NMR spectrum by a HSQC experiment. The ^{11}B NMR spectrum evidenced complete consumption of HBpin and comprised a major singlet resonance at δ 26.0 ppm, consistent with analogous data reported for the range of *N*-borylated methylamines described in our earlier study of isocyanate hydroboration.[65] Stimulated by this outcome, this reactivity was extended to the isolated magnesium and calcium *N*-alkyl; and aryl formamidate derivatives, **18** - **25**. These results are summarised in Table 3.

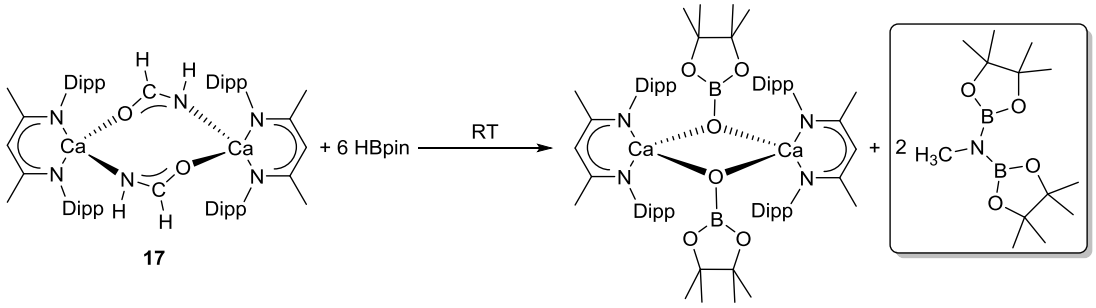

Scheme 11: Postulated stoichiometric reduction of complex **17** with three equivalents of HBpin to yield a calcium boryloxide and $(pinB)_2NCH_3$.

.

Table 3: Addition of four equivalents of HBpin to compounds **18** – **25** to provide the respective $(pinB)N(R/Ar)CH_3$ products.

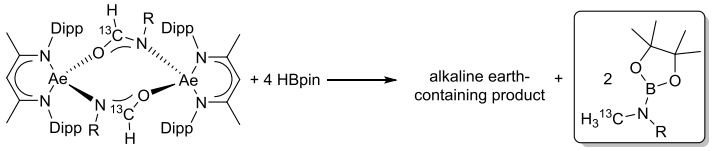

Entry	Compd.	Ae	Product	Time (h)	Temp. (°C)	Conv. (%)[a]
1	**18**	Mg	*n*-BuN(CH_3)(Bpin)	24	60	99
2	**20**	Mg	*i*-PrN(CH_3)(Bpin)	48	60	99
3	**21**	Mg	Ph(CH_2)$_2$N(CH_3)(Bpin)	24	80	87
4	**22**	Mg	DippN(CH_3)(Bpin)	72	60	99
5	**19**	Ca	*n*-BuN(CH_3)(Bpin)	2	25	87
6	**23**	Ca	*t*-BuN(CH_3)(Bpin)	<1	25	99
7	**24**	Ca	Ph(CH_2)$_2$N(CH_3)(Bpin)	<1	25	90
8	**25**	Ca	DippN(CH_3)(Bpin)	12	60	99

[a] Determined by ^1H NMR spectroscopy

Marked variations in reactivity were observed across the various magnesium and calcium formamidates. Compounds **18** and **20** – **22** required elevated temperatures and extended reaction times

to provide high (*ca.* ~ 90%) conversions to the *N*–methyl amine products, whereas the calcium derivatives **19**, **23** and **24** were observed to undergo facile reduction at ambient temperature and only the most sterically encumbered *N*-Dipp derivative **25** required heating to effect commensurate conversion.

To further explore the origin of these observations, stoichiometric reactions were undertaken with the calcium compounds **19** and **23** – **25**. Addition of one equivalent of HBpin to **19**, **23** and **24** led to the rapid and complete consumption of the borane reagent to provide a distribution of starting material and the respective *N*–^{13}C methyl amine at the first point of analysis. A further reaction between **25** and a single molar equivlent of HBpin carried out in hexane cooled to –35 °C, however, induced crystallization of colorless plate crystals of compound **27** which were suitable for X–ray diffraction analysis. The results of this analysis are shown in Figure 16, while details of the analysis and selected bond length and angle data are provided in table 2 and the figure caption respectively. The solid state structure of **27** is comparable to that of compound **25** in comprising a solitary *β*–diketiminate ligand, which is bound in a bidentate fashion to Ca1. Three *N*–Dipp formamidate ligands bind via μ_2-bridging interactions through their oxygen atoms (O1, O2 and O3) to Ca1, completing a trigonal bipyramidal geometry for Ca1. The second calcium center (Ca2) also has two *N*–Dipp formamidates bound in a κ^2–fashion from both the oxygen (O2 and O3) and the nitrogen (N4 and N5) atoms of each ligand and two further contacts provided by a coordinated oxygen (O4) from a pinacolborane fragment, which has effectively inserted into the Ca–N bond of the remaining formamidate ligand. The boron–bound hydride was readily located and freely refined, clearly demonstrating a Ca–H interaction in the solid state. The constitution of the formamidatoborate component of its structure is clearly reminiscent of the borate species, [{HC(Me)NDipp}$_2$Mg{OC(H)NDipp(HBpin)], which was identified as a key intermediate during the magnesium-mediated hydroboration of isocyanates.[65, 69] Although the reactivity of compound **27** has not been investigated further, we suggest that the reduction of the formamidate species derived through the carbonylation of alkaline earth primary amides occurs through a sequence of reaction steps which is otherwise analogous to those depicted in Scheme 10(a).

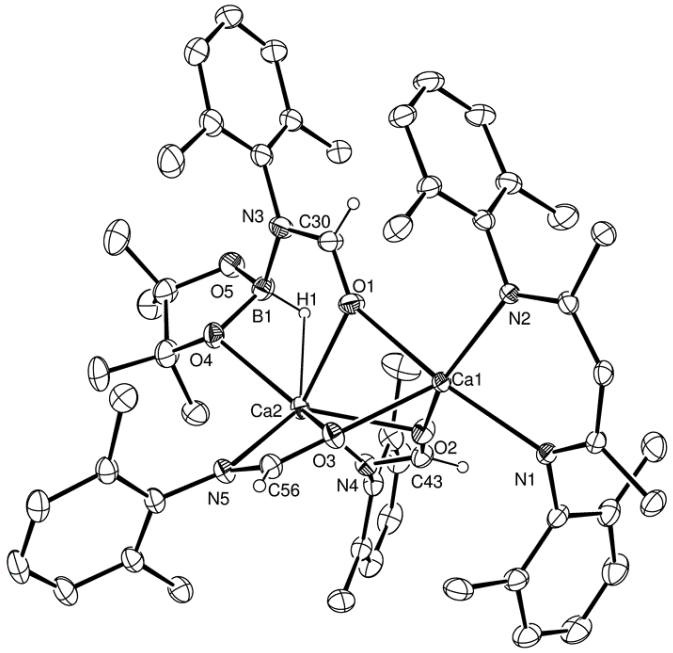

Figure 16: ORTEP representation of **27** with thermal ellipsoids at 25%. *Iso*-propyl groups and hydrogen atoms except hydrogens attached to C30, C43, C56 and B1, have been removed for clarity. Selected bond lengths (Å) and bond angles (°): Ca1–O1 2.503(2), Ca1–O2 2.228(2), Ca1–O3 2.224(2), Ca1–N1 2.389(2), Ca1–N2 2.353(2), Ca2–O1 2.376(2), Ca2–O2 2.412(2), Ca2–O3 2.503(2), Ca2–O4 2.293(3), Ca2–N4 2.487(2), Ca2–N5 2.455(2), O1–C30 1.268(4), O2–C43 1.281(3), O3–C56 1.286(3), B1–N3 1.685(6), N3–C30 1.267(4), N4–C43 1.295(4), N5–C56 1.292(4). O1–Ca1–O2 75.72(7), N1–Ca1–O1 167.01(8), N2–Ca1–O1 100.72(7), N3–C30–O1 123.9(3), N4–C43–O2 121.0(3), N5–C56–O3 121.3(3), C30–N3–B1 116.2(3), O4–B1–N3 105.5(3), O5–B1–O5 106.3(4), B1–O4–Ca2 92.4(2).

On the basis of these observations a catalytic cycle for the HBpin-derived hydrodeoxygenation of formamidates generated from amine carbonylation with compounds **4** or **11** may be readily envisaged (Scheme 10(b), *Cycle 1*). A protonolysis reaction between an alkaline earth hydride and an amine (RNH_2, R = Alkyl, Aryl or H) will generate dihydrogen and a *β*–diketiminato alkaline earth amide. Subsequent carbonylation with CO will generate a formamidate intermediate, whereupon a reductive sequence of deoxygenative hydroboration steps completely analogous to those depicted in Scheme 10(a) will ultimately result in methyl amine production and the regeneration of the alkaline earth hydride which is primed for the propagation of the onward trajectory of the catalysis through reaction with a further molecule of RNH_2.

The stoichiometric reactivity described above demonstrates the feasibility of all the reaction steps depicted in Scheme 10(b) for the formylation and deoxygenative methylation of amines and the direct utilization of carbon monoxide as a C_1 carbon source. Our initial attempts to extend this reactivity to a catalytic regime, however, have been thwarted by the previously reported facility of alkaline earth reagents to catalyze the homogeneous dehydrocoupling of HBpin and amines (Scheme 10(b), *Cycle 2*)

and the comparatively limited solubility of CO in hydrocarbon solvents under the 1 atmosphere conditions applied during the catalysis.[70] We are, thus, continuing to develop this novel alkaline earth-centered formylation, homologation and reduction reactivity under higher CO pressures and will report our observations in future publications.[45]

Experimental Section

General Experimental Procedures. All reactions dealing with air– and moisture–sensitive compounds were carried out under an argon atmosphere using standard Schlenk line and glovebox techniques in a MBraun Labmaster glovebox at O_2, H_2O <0.1 ppm. NMR experiments using air–sensitive compounds were conducted in J. Young's tap NMR tubes prepared and sealed in a glovebox under argon. All NMR data were acquired on a Bruker 300 UltrashieldTM for ^1H (300 MHz) and $^{13}C\{^1H\}$ (75.48 MHz) spectra at room temperature or a Bruker 400 UltrashieldTM for ^1H (400 MHz) and $^{13}C\{^1H\}$ (125.76 MHz) spectra. $^1H/^{13}C$ NMR spectra were referenced using residual solvent resonances. Elemental analyses of all moisture– and air–sensitive compounds were performed by Mr Stephen Boyer of London Metropolitan Enterprises. Solvents for air– and moisture–sensitive reactions were provided by an Innovative Technology Solvent Purification System. C_6D_6 and toluene–d_8 were purchased from Fluorochem and dried over molten potassium prior to vacuum transfer into a sealed ampoule and storage in the glovebox under argon. CO was purchased from BOC. Di–*n*–butylmagnesium (1.0 M solution in *n*–heptane), pinacolborane (HBpin), phenylsilane ($PhSiH_3$) and ^{13}CO were purchased from Sigma–Aldrich Ltd. Organic amines were purchased from the same supplier and dried over P_2O_5 before either distillation or vacuum transfer. Compounds **4**, **9** and **11** were synthesized by literature procedures.[45, 46]

Synthesis of [(HC{(*t*-Bu)CN(2,6–^{i}PrC$_6$H$_3$)}$_2$Mg)$_2$(OHC=CHO)], 10. A solution of compound **9** (70 mg, 0.15 mmol) in 0.5 ml toluene was freeze–thaw degassed and exposed to ~1 atm of CO. The reaction flask was resealed and left at room temperature for two hours before the solution was interrogated by NMR spectroscopic analysis, which revealed stoichiometric conversion to compound **10**. The solvent was then removed *in vacuo* and the resultant pale yellow solid was redissolved in *n*–pentane. Storage of this solution at −30 ºC for two days afforded crystals of compound **10** suitable for single crystal X–ray diffraction analysis. NMR Yield: 100% (Isolated Yield: 72%, 50 mg). ^1H NMR (d_8–tol.): δ 7.05 – 7.02 (6H, br. m, Ar–*H*), 5.39 (1H, s, C*H*), 5.16 (1H, s, O(*H*C=C*H*)O), 3.63, 3.34, 3.23, 2.87 (4H, br. m., C*H*(CH$_3$)$_2$), 1.31 (24H, br. m, CH(C*H*$_3$)$_2$), 1.16 (18H, br. m, NC(C(C*H*$_3$)$_3$)CH). $^{13}C\{^1H\}$ NMR (d_8–tol., 125.76 MHz): δ 171.6, 169.0 (N*C*(CH$_3$)CH), 148.1, 142.9, (*C*–Ar), 130.8 (O(H*C*=*C*H)O), 124.2, 123.9, 123.4 (*C*–Ar), 97.2 (NC(C(CH$_3$)$_3$)*C*H), 44.8 (NC(*C*(CH$_3$)$_3$)CH), 33.7 (NC(C(*C*H$_3$)$_3$)CH), 28.8 (bs, *C*H(CH$_3$)$_2$), 24.9 (bs, CH(*C*H$_3$)$_2$). Despite multiple attempts, an accurate microanalysis could not be obtained for this compound.

Synthesis of [(HC{(Me)CN(2,6–^{i}PrC$_6$H$_3$)}$_2$Ca)$_2$(OHC=CHO)], 12. A solution of compound **11** (50 mg, 0.09 mmol) in 0.5 ml toluene was freeze–thaw degassed and exposed to ~1 atm of CO. The reaction flask was resealed and left at room temperature for 1 hour before the solution was interrogated by NMR spectroscopic analysis, which revealed stoichiometric conversion to compound **12**. Storage of this solution at room temperature for two days afforded crystals of compound **12** suitable for single crystal X–ray diffraction analysis. NMR Yield: 100% (Isolated Yield: 92%, 64 mg). ^{1}H NMR (d_8–tol.): δ 7.06 – 6.97 (6H, m, Ar*H*), 5.00 (1H, s, O(*H*C=C*H*)O), 4.65 (1H, s, C*H*), 3.38 (THF), 3.08 (4H, m., $^{3}J_{HH}$ = 6.40 Hz, C*H*(CH$_3$)$_2$), 1.63 (6H, s, NC(C*H*$_3$)CH), 1.40 (THF), 1.19 (12H d, $^{3}J_{HH}$ = 6.40 Hz, CH(C*H*$_3$)$_2$). ^{13}C{^{1}H} NMR (d_8–tol., 125.76 MHz): δ 165.3 (N*C*(CH$_3$)CH), 148.0 (*ipso*–Ar), 142.3 (*o*–Ar), 131.9 (O(H*C*=*C*H)O), 124.1 (*p*–Ar), 123.5 (*m*–Ar), 93.6 (NC(CH$_3$)*C*H), 69.1 (THF), 28.7, 26.0 (N*C*H(CH$_3$)$_2$), 25.4 (THF), 25.1, 24.9 (CH(*C*H$_3$)$_2$). Anal. Calcd. for C$_{68}$H$_{100}$Ca$_2$N$_4$O$_4$: C, 73.07; H, 9.02; N, 5.01%. Found: C, 74.23; H, 9.10; N, 4.89%.

Catalytic reduction of CO (representative procedure). In a glovebox, to a vial containing compound **4** or **11**, (0.02 mmol, 10 mg), was added toluene–d_8 (0.5 mL) followed by PhSiH$_3$ (0.2 mmol, 27.8 µl). The resultant solution was transferred to a NMR tube equipped with a J. Young's tap, which was sealed and removed from the glovebox. The solution was then freeze pumped thaw degassed to remove argon, exposed to 1 atmosphere of ^{13}CO, resealed and warmed to 60 °C. ^{1}H and NMR analysis was performed at regular intervals and conversions were analyzed by ratios of starting material to product, with products identified by comparison to literature values.[43]

Synthesis of [HC{(Me)CN(2,6–^{i}PrC$_6$H$_3$)}$_2$CaNH$_2$(dioxane)]$_2$, 16. To a stirred solution of **11** (500 mg, 0.94 mmol) in toluene was added 0.5 M solution of ammonia in dioxane (1.88 ml). The resultant solution was stirred overnight. The solvent was then removed *in vacuo* to yield an off white powder (430 mg, 81%). A saturated toluene solution of **16** stored at –35°C over night yielded large colourless needles suitable for an X–ray diffraction experiment. ^{1}H NMR (d_8–tol.): δ 7.00 (6H, s, Ar–*H*), 4.72 (1H, s, C*H*), 3.35 (dioxane), 3.15 (4H, m., $^{3}J_{HH}$ = 6.78 Hz, C*H*(CH$_3$)$_2$), 1.63 (6H, s, NC(C*H*$_3$)CH), 1.13 (12H d, $^{3}J_{HH}$ = 6.78 Hz, CH(C*H*$_3$)$_2$), 1.03 (12H d, $^{3}J_{HH}$ = 6.78 Hz, CH(C*H*$_3$)$_2$) –1.54 (2H, bs, NH$_2$). ^{13}C{^{1}H} NMR (d_8–Tol, 125.76 MHz): δ 165.3 (N*C*(CH$_3$)CH), 147.8, 142.2, 124.6, 124.2 (*C*–Ar), 94.3 (NC(CH$_3$)*C*H), 67.5 (dioxane) 28.6 (*C*H(CH$_3$)$_2$), 25.3, 24.7 (CH(*C*H$_3$)$_2$). Anal. Calcd. for C68H106Ca2N6O4: C, 72.58; H, 9.41; N, 7.69% Found: C, 72.45; H, 9.85; N, 7.40%

Synthesis of [(HC{(Me)CN(2,6–^{i}PrC$_6$H$_3$)}$_2$Ca(OC(H)NH)]$_2$, 17. A solution of compound **16** (70 mg, 0.15 mmol) in 0.5 ml toluene was freeze–thaw degassed and exposed to 1 atmosphere of CO. The reaction flask was resealed and left at room temperature for two hours before the solution was

interrogated by NMR spectroscopic analysis, which revealed stoichiometric conversion to compound **17**. The solvent was then removed *in vacuo* and the resultant pale yellow solid was re–dissolved in *n*–hexane. Storage of this solution at −30 ºC for two days afforded crystals of compound **17** suitable for single crystal X–ray diffraction analysis. . NMR Yield: 80% (Isolated Yield: 69%, 48 mg). ^{1}H NMR (d_8–tol., 500 MHz): δ 7.01 (6H, 3, Ar–*H*), 6.61 (1H, dd, $^{1}J_{HC}$ = 183.1, $^{3}J_{HH}$ = 6.1 Hz, ^{13}C*H*) 4.65 (1H, s, C–*H*), 3.44 (THF), 3.15 (4H, br. sept., $^{3}J_{HH}$ = 6.65 Hz, C*H*(CH$_3$)$_2$), 1.63 (6H, s, NC(C*H*$_3$)CH), 1.43 (THF), 1.19 (12H br. d, CH(C*H*$_3$)$_2$), 1.02 (12H br. d, CH(C*H*$_3$)$_2$) –1.93 (1H, br. s, NH$_2$). ^{13}C{^{1}H} NMR (d_8–tol., 125.76 MHz): 174.3 N*C*(H)O, 165.1 (N*C*(CH$_3$)CH), 148.2, 143.1, 142.3, 142.0, 120.2, 124.3, 124.0 (*C*–Ar), 94.0 (NC(CH$_3$)*C*H), 68.8, 67.53 (dioxane), 29.0, 28.46 (*C*H(CH$_3$)$_2$), 26.0, 25.6, 25.0, 24.8, 23.8 (CH(*C*H$_3$)$_2$). Anal. Calcd. for $C_{60}H_{86}Ca_2N_6O_2$: C, 71.81; H, 8.64; N, 8.37%. Found: C, 73.88; H, 9.14; N, 7.71%.

General procedure for the synthesis of [HC{(Me)CN(2,6–^{i}PrC$_6$H$_3$)}$_2$Ae(OC(H)NR)]$_2$. (Ae = Mg or Ca. R = aryl or alkyl). A solution of compound **4** or **11** (30 mg, 0.067 or 0.056mmol) in 0.5 ml toluene with two equivalents of a primary amine were mixed in a J. Young tube and left for one hour. The solution was then interrogated by NMR spectroscopy to ensure complete conversion to the corresponding amide. The solution was then freeze–thaw degassed and exposed to ~1 atm. of CO and the reaction followed by NMR until complete conversion the formamidate product.

Synthesis of [HC{(Me)CN(2,6–^{i}PrC$_6$H$_3$)}$_2$Mg(OCH=N*n*-Bu)]$_3$, 18. Reaction reached full conversion within 24 hours at 60ºC temperature. Cooling of this solution to room temperature afforded crystals of compound **18** suitable for single crystal X–ray diffraction analysis. NMR Yield: 99% (Isolated Yield: 94%, 28 mg). ^{1}H NMR (d_8–tol., 300 MHz): δ 7.87, (0.25H, d, $^{1}J_{CH}$ = 177.4 Hz, NC(*H*)O), (0.75H, d, $^{1}J_{CH}$ = 182.9 Hz, NC(*H*)O), 7.35 (1H, d, $^{1}J_{CH}$ = 177.4 Hz, NC(*H*)O), 7.15 – 7.02 (5H, br. m, Ar–*H*), 6.98 (1H, br. m, Ar–*H*), 4.82, 4.70 (1H, s, C–*H*), 3.38 (1H, br. sept., C*H*(CH$_3$)$_2$), 3.10 (3H, br. sept., C*H*(CH$_3$)$_2$), 1.60 (6H, s, NC(C*H*$_3$)CH), 1.52 (3H, br. m, CH(C*H*$_3$)$_2$), 1.24–1.13 (21H, br. m, CH(C*H*$_3$)$_2$), 1.02 (3H, t, $^{3}J_{HH}$ = 7.16 Hz, CH$_2$C*H*$_3$), CH$_2$C*H*$_3$). 0.87 (2H, br. m, CH$_2$C*H*$_3$), 0.42–0.28 (4H, br. m, NC*H*$_2$C*H*$_2$). ^{13}C{^{1}H} NMR (d_8–tol, 125.76 MHz): δ 171.9, 1.65.0 (N*C*(H)O), due to the poor solubility of **18**, no other meaningful ^{13}C{^{1}H} NMR data could be obtained. Anal. Calcd. for $C_{34}H_{51}MgN_3O$: C, 75.33; H, 9.48; N, 7.75%. Found: C, 75.36; H, 9.12; N, 7.14%.

Synthesis of [HC{(Me)CN(2,6–^{i}PrC$_6$H$_3$)}$_2$Ca(OCH=N*n*-Bu)]$_2$, 19. Reaction reached full conversion within an hour at room temperature. Storage of this solution at room temperature for two days afforded crystals of compound **19** suitable for single crystal X–ray diffraction analysis. NMR Yield: 99% (Isolated Yield: 76%, 23 mg). ^{1}H NMR (d_8–THF, 300 MHz): δ 7.09 (6H, br. m, Ar–*H*), 5.92 (1H, d, $^{1}J_{HC}$ = 179.48 Hz, NC(*H*)O), 4.91 (1H, s, C–*H*), 3.15 (4H, sept., $^{3}J_{HH}$ = 6.92 Hz C*H*(CH$_3$)$_2$), 1.69 (6H,

s, NC(CH_3)CH), 1.55 (3H, br. m, CH(CH_3)$_2$), 1.20 (12H, d, $^3J_{HH}$ = 7.16 Hz, CH(CH_3)$_2$), 1.20 (12H, d, $^3J_{HH}$ = 7.16 Hz, CH(CH_3)$_2$), 0.85 (2H, NCH_2CH$_2$), CH$_2$CH_3).^{13}C{^{1}H} NMR (d_8–THF, 125.76 MHz): δ 170.9 (N*C*(H)O), due to the poor solubility of **19**, no other meaningful ^{13}C{^{1}H} NMR data could be obtained. Anal. Calcd. for $C_{38}H_{59}CaN_3O_2$: C, 72.45; H, 9.44; N, 6.67%. Found: C, 73.05; H, 9.62; N, 6.83%.

Synthesis of [(HC{(Me)CN(2,6–^{i}PrC$_6$H$_3$)}$_2$MgOC(H)N^{i}Pr)]$_2$, 20. Reaction reached full conversion within an hour at room temperature. Storage of this solution at RT for two days afforded crystals of compound **20** suitable for single crystal X–ray diffraction analysis. NMR Yield: 99% (Isolated Yield: 68%, 20 mg). ^{1}H NMR (d_8–THF, 300 MHz): δ 7.09 (6H, br. m, Ar–*H*), 5.92 (1H, d, $^1J_{HC}$ = 179.48 Hz, NC(*H*)O), 4.91 (1H, s, C–*H*), 3.15 (4H, sept., $^3J_{HH}$ = 6.92 Hz C*H*(CH$_3$)$_2$), 1.69 (6H, s, NC(CH_3)CH), 1.55 (3H, br. m, CH(CH_3)$_2$), 1.20 (12H, d, $^3J_{HH}$ = 7.16 Hz, CH(CH_3)$_2$), 1.20 (12H, d, $^3J_{HH}$ = 7.16 Hz, CH(CH_3)$_2$), 0.85 (2H, NCH_2CH$_2$), CH$_2$CH_3).^{13}C{^{1}H} NMR (d_8–THF, 125.76 MHz): δ 170.9 (N*C*(H)O), due to the poor solubility of **20**, no other meaningful ^{13}C{^{1}H} NMR data could be obtained. Anal. Calcd. for C66H98Mg2N6O2: C, 75.06; H, 9.35; N, 7.96%. Found: C, 75.21; H, 9.71; N, 7.58%.

Synthesis of [(HC{(Me)CN(2,6–^{i}PrC$_6$H$_3$)}$_2$MgOC(H)NCH$_2$CH$_2$C$_6$H$_5$)]$_2$, 21. The reaction flask was resealed and left at 100 °C for 12h. Inspection of the reaction flask after 12 hours reveiled the formation of X–ray quality crystals. Isolation of this solid provided an 80% isolated yield. **21** was extremely insoluble and NMR characterization was carried out in a saturated THF solution. NMR Yield: 99% (Isolated Yield: 52%, 15 mg). ^{1}H NMR (d_8–THF, 300 MHz): δ 7.84 (1H, d, $^1J_{HC}$ = 176.07 Hz NC(*H*)O), 7.81 (1H, d, $^1J_{HC}$ = 180.48 Hz NC(*H*)O), 7.24 – 7.21 (5H, br. m, Ar–*H*), 7.07 – 7.04 (12H, br. m, Ar–*H*), 6.98 – 6.95 (3H, br. m, Ar–*H*), 6.91 – 6.88 (4H, br. m, Ar–*H*) 4.92, 4.86 (1H, s, C–*H*), 3.24, 3.15 (4H, sept, $^3J_{HH}$ = 6.85 Hz, C*H*(CH$_3$)$_2$), 2.80, 2.66, (2H, bt, $^3J_{HH}$ = 7.34 Hz, NCH_2CH$_2$), 2.49, 1.92 (2H, bt, $^3J_{HH}$ = 7.34 Hz, NCH$_2$CH_2), 1.81, 1.65 (6H, s, NC(CH_3)CH), 1.26 (6H, d, $^3J_{HH}$ = 6.85 Hz, CH(CH_3)$_2$), 1.22 – 1.19 (24H, br. m, CH(CH_3)$_2$), 1.07 (6H, d, $^3J_{HH}$ = 6.85 Hz, CH(CH_3)$_2$), 1.02 (6H, d, $^3J_{HH}$ = 6.85 Hz, CH(CH_3)$_2$), 0.17 (6H, d, $^3J_{HH}$ = 6.85 Hz, CH(CH_3)$_2$). ^{13}C{^{1}H} NMR (d_8–THF, 125.76 MHz): δ 174.2 (N*C*(H)O), 172.52 (N*C*(CH$_3$)CH), 169.1 (N*C*(H)O), 143.2, 129.6, 129.4, 127.0, 126.2, 125.7, 124.7, 124.2, 113.9, 123.7 (*C*–Ar), 95.2 (NC(CH$_3$)*C*H), 29.2, 29.1 (N*C*H$_2$CH$_2$), 28.9, 28.8, (NCH$_2$*C*H$_2$), 24.9 (*C*H(CH$_3$)$_2$), 24.6, 24.2 (CH(*C*H$_3$)$_2$), 24.1 (*C*H(CH$_3$)$_2$), 23.6, 23.4 (CH(*C*H$_3$)$_2$). Despite repeated attempts, no accurate microanalysis could be obtained for this compound.

Synthesis of [(HC{(Me)CN(2,6–^{i}PrC$_6$H$_3$)}$_2$MgOC(H)N(2,6–^{i}PrC$_6$H$_3$)]$_2$, 22. The reaction flask was resealed and left at room temperature for one hour before the solution was interrogated by NMR spectroscopic analysis. The revealed stoichiometric conversion to compound **22**. ^{1}H NMR (d$_8$–tol, 300 MHz): δ 7.92 (1H, s, NC(*H*)O), 7.06 (6H, bs, Ar–*H*), 6.90 (3H, s, Ar–*H*), 4.96 (1H, s, C–*H*), 3.44 (2H,

bm, C*H*(CH_3)$_2$), 3.17 (2H, bm, C*H*(CH_3)$_2$), 1.98 (2H, m, $^3J_{HH}$ = 6.78 Hz, C*H*(CH_3)$_2$), 1.66 (6H, s, NC(C*H*$_3$)CH), 1.33 (6H, bm, CH(C*H*$_3$)$_2$), 1.11 (12H, d, $^3J_{HH}$ = 6.78 Hz, CH(C*H*$_3$)$_2$), 0.96 (6H, bm, CH(C*H*$_3$)$_2$), 0.80 (6H, d, $^3J_{HH}$ = 6.78 Hz, CH(C*H*$_3$)$_2$). ^{13}C{^{1}H} NMR (d_8–tol, 125.76 MHz): δ 175.0 (N*C*(H)O),169.7 (N*C*(CH_3)CH), 143.9, 143.5, 140.3, 125.95, 125.40, 124.3, 122.9 (*C*–Ar), 95.1 (NC(CH_3)*C*H), 28.1, 27.8 (N*C*H(CH_3)$_2$), 24.7, 23.8 (CH(*C*H_3)$_2$). Despite multiple attempts, a meaningful microanalysis could not be obtained for this compound.

Synthesis of [HC{(Me)CN(2,6–*i*-PrC_6H_3)}$_2$Ca(OCH=N*t*-Bu)]$_2$, 23. The reaction flask was resealed and left at room temperature for one hour before the solution was interrogated by NMR spectroscopic analysis. This revealed stoichiometric conversion to compound **23**. NMR Yield: 99% (Isolated Yield: 91%, 27 mg). ^{1}H NMR (d_8–tol., 500 MHz): δ 8.06 (1H, d, $^1J_{CH}$ = 179.34 Hz, NC(*H*)O), 7.13 – 7.04 (10H, m, Ar–*H*), 4.72 (1H, s, C–*H*), 3.39, 3.03 (1H, sept., $^3J_{HH}$ = 6.78 Hz, C*H*(CH_3)$_2$), 2.95 (2H, sept., $^3J_{HH}$ = 6.78 Hz, C*H*(CH_3)$_2$), 1.58, 1.55 (3H, s, NC(C*H*$_3$)CH), 1.30 (3H d, $^3J_{HH}$ = 6.78 Hz, CH(C*H*$_3$)$_2$), 1.21, 1.19 (18H bd, CH(C*H*$_3$)$_2$), 1.13 (9H, s, C(C*H*$_3$)$_3$), 0.42 (3H d, $^3J_{HH}$ = 6.78 Hz, CH(C*H*$_3$)$_2$). ^{13}C{^{1}H} NMR (d_8–tol., 125.76 MHz): δ 167.3 O*C*(H)N, 165.7 (N*C*(CH_3)CH), 136.7, 129.6, 128.6, 125.8, 124.6, 124.4, 123.9, 123.7 (*C*–Ar), 93.2 (NC(CH_3)*C*H), 53.4 (N*C*(CH_3)$_3$), 32.4, 32.1, 32.0, 29.0 (N*C*H(CH_3)$_2$), 28.8 (CH(*C*H_3)$_2$), 27.7, 25.9, 25.1, 24.9, 24.7, 24.4 (NC(*C*H_3)CH), 24.1 (NC(*C*H_3)$_3$), 23.8 (NC(*C*H_3)CH), 23.5 (CH(*C*H_3)$_2$). Anal. Calcd. for C76H118Ca2N6O4: C, 72.45; H, 9.44; N, 6.67%. Found: C, 71.93; H, 8.94; N, 4.55%.

Synthesis of [HC{(Me)CN(2,6–^{i}PrC_6H_3)}$_2$Ca(OCH=NCH_2CH_2C$_6H_5$)]$_2$, 24. The reaction flask was resealed and left at room temperature for one hour before the solution was interrogated by NMR spectroscopic analysis. This revealed stoichiometric conversion to compound **24**. ^{1}H NMR (d_8–tol., 500 MHz): δ 7.45 (1H, d, $^1J_{CH}$ = 180.09 Hz, NC(*H*)O), 7.13 – 7.05 (10H, m, Ar–*H*), 4.74 (1H, s, C–*H*), 3.16 (3H, br. m., C*H*(CH_3)$_2$), 2.95 (1H, sept., $^3J_{HH}$ = 6.76 Hz, C*H*(CH_3)$_2$), 2.85 (qt., $^3J_{HH}$/$^3J_{CH}$ = 7.16 Hz, CH_2CH_2N), 1.63 (5H, s, NC(C*H*$_3$)CH), 1.55 (1H, s, NC(C*H*$_3$)CH), 1.21, 1.20 (12H d, $^3J_{HH}$ = 6.76 Hz, CH(C*H*$_3$)$_2$), 0.91 (3H, t., $^3J_{HH}$ = 7.16 Hz, CH_2CH_3). ^{13}C{^{1}H} NMR (d_8–tol., 125.76 MHz): δ 168.8 O*C*(H)N, 165.9 (N*C*(CH_3)CH), 146.5, 142.1, 136.7, 124.7, 124.2, 123.7 (*C*–Ar), 93.7 (NC(CH_3)*C*H), 50.2 (NCH_2*C*H_2Ar), 35.0 (N*C*H_2CH_2Ar), 29.0, 28.7 (N*C*H(CH_3)$_2$), 25.5, 24.8, 24.6, 24.1, 23.5 (CH(*C*H_3)$_2$). Accurate microanalytical data could not be obtained for this compound.

Synthesis of [HC{(Me)CN(2,6–^{i}PrC_6H_3)}$_2$Ca(OCH=NDipp)$_3$Ca(THF)THF], 25. The reaction flask was resealed and heated at 60 °C for one hour before the solution was interrogated by NMR spectroscopic analysis. This revealed stoichiometric conversion to compound **25**. ^{1}H NMR (d_8–tol., 500 MHz): δ 7.41 (1H, d, $^1J_{CH}$ = 183.41 Hz, NC(*H*)O), 7.17 – 6.77 (9H, m, Ar–*H*), 4.95 (1H, s, C–*H*), 3.54 THF, 3.44 (1H, sept., $^3J_{HH}$ = 6.85 Hz, C*H*(CH_3)$_2$), 3.11 (1H, sept., $^3J_{HH}$ = 6.85 Hz, C*H*(CH_3)$_2$), 2.98 (1H,

sept., $^3J_{HH}$ = 6.85 Hz, C*H*(CH_3)$_2$), 2.58 (1H, sept., $^3J_{HH}$ = 6.85 Hz, C*H*(CH_3)$_2$), 1.83, 1.71, 1.57 (2H, s, NC(C*H*$_3$)CH), 1.51 (3H d, $^3J_{HH}$ = 6.85 Hz, CH(C*H*$_3$)$_2$), 1.73 (4H d, $^3J_{HH}$ = 6.85 Hz, CH(C*H*$_3$)$_2$), 1.28 (3H d, $^3J_{HH}$ = 6.85 Hz, CH(C*H*$_3$)$_2$), 1.23 (7H d, $^3J_{HH}$ = 6.85 Hz, CH(C*H*$_3$)$_2$), 1.19 (11H d, $^3J_{HH}$ = 6.85 Hz, CH(C*H*$_3$)$_2$), 1.00, 0.97 (2H d, $^3J_{HH}$ = 6.85 Hz, CH(C*H*$_3$)$_2$), 0.47, 0.43 (2H d, $^3J_{HH}$ = 6.85 Hz, CH(C*H*$_3$)$_2$). ^{13}C{^{1}H} NMR (d_8–tol., 125.76 MHz): δ 174.2 (N*C*(CH_3)CH), 171.2 O*C*(H)N, 151.1, 149.3, 145.7, 144.5, 143.6, 142.5, 142.1, 141.9, 141.4, 140.8, 124.7, 124.4, 124.3, 124.1, 123.6, 123.2 (*C*–Ar), 94.9 (NC(CH_3)*C*H), 68.8 THF, 32.4, 28.7, 28.4, 28.1, 27.8, 27.1, 26.2, 26.1 (N*C*H(CH_3)$_2$), 25.9, 25.6 (CH(*C*H_3)$_2$), 25.4 THF, 24.9, 24.70, 24.06, 23.5, 22.9 (CH(*C*H_3)$_2$). Accurate microanalytical data could not be obtained for this compound.

Synthesis of [HC{(Me)CN(2,6–^{i}PrC$_6$H$_3$)}$_2$MgOHCN(Me)C$_6$H$_5$)]$_2$, 26. One atmosphere of ^{13}CO was added to a J Young NMR tube containing a degassed solution of compound **4** (0.067 mmol) and *N*–methyl aniline (0.067 mmol) in toluene. The reaction was left at room temperature and interrogated by NMR spectroscopy. Multinuclear NMR spectroscopy could not identify starting material from product with any meaningful level of confidence. Incipient crystallisation directly from the J Youngs tube afforded **26** as X–ray quality crystals. NMR yield 68% (Isolated Yield: 8 mg). ^{1}H NMR (d_8–Tol): δ 7.21–7.18 (3H, m, Ar–*H*), 7.14–7.13 (2H, m, Ar–*H*), 7.00–6.94 (2H, t, $^3J_{HH}$ = 7.16 Hz Ar–*H*), 6.60–6.55 (1H, t, $^3J_{HH}$ = 7.16 Hz Ar–*H*), 5.95–5.92 (2H, d, $^3J_{HH}$ = 7.16 Hz Ar–*H*), 4.99 (1H, s, C–*H*), 3.15 (4H, spt., $^3J_{HH}$ = 6.78 Hz, C*H*(CH_3)$_2$), 2.18 (3H, s, NC*H*$_3$) 1.69 (6H, s, NC(C*H*$_3$)CH), 1.20, 1.75 (24H d, $^3J_{HH}$ = 6.78 Hz, CH(C*H*$_3$)$_2$). ^{13}C{^{1}H} NMR (d_8–Tol, 125.76 MHz): δ 235.7 (O*C*N(CH_3)Ph). No other NMR spectroscopic or microanalytical data could be obtained for this compound.

Synthesis of [H$_3$^{13}CN(Bpin)$_2$]

Addition of 4,4,5,5,–tetramethyl–1,3,2–dioxaborolane (0.402 mmol) to a J Youngs tube containing a solution of compound **17** (0.067 mmol) in toluene. The reaction was left at room temperature and probed by NMR spectroscopy after initiation of the reaction. ^{1}H NMR (d_8–THF, 500 MHz): δ 2.98 (3H, d, $^1J_{HC}$ = 136.5 Hz N^{13}C*H*$_3$), 2.18, 2.08, (12H, s, OC(CH_3)$_2$). ^{13}C{^{1}H} NMR (d_8–THF, 125.76 MHz): δ 79.0 (O*C*(CH_3)$_2$), 34.4 (N*C*H$_3$), 28.7 (OC(*C*H_3)$_2$). ^{11}B NMR (d_8–THF, 125.76 MHz): δ 27.3.

Synthesis of [HC{(Me)CN(2,6–^{i}PrC$_6$H$_3$)}$_2$Ca(OCH=NDipp)$_3$(HBpin)Ca], 27. Addition of 4,4,5,5,–tetramethyl–1,3,2–dioxaborolane (0.067 mmol) to a J Young tube containing a solution of compound **25** (0.067 mmol) in toluene. The reaction was left at room temperature and probed by NMR spectroscopy after initiation of the reaction. NMR Yield: 71% (Isolated Yield: 9 mg). ^{1}H NMR (d_8–Tol, 500 MHz): δ 7.13 – 7.03 (8H, m, Ar–*H*, OC(*H*)N), 6.94 – 6.89 (4H, m, Ar–*H*), 6.74 – 6.71 (1H, m, Ar–*H*), 4.94 (1H, s, C–*H*), 3.39–3.29 (3H, b sept., C*H*(CH_3)$_2$), 3.24–3.17 (3H, b sept., C*H*(CH_3)$_2$), 3.16–3.12 (1H, b sept., C*H*(CH_3)$_2$), 3.01–2.93 (2H, b sept., C*H*(CH_3)$_2$), 2.60–2.56 (3H, sept., $^3J_{HH}$ = 6.85 Hz,

C*H*(CH_3)$_2$), 1.82 (2H, s, NC(C*H*$_3$)CH), 1.75 (1H, s, NC(C*H*$_3$)CH), 1.65 (1H, s, NC(C*H*$_3$)CH), 1.56 (2H, s, NC(C*H*$_3$)CH), 1.36 (6H, d, $^3J_{HH}$ = 6.85 Hz, CH(C*H*$_3$)$_2$), 1.30–1.13 (40H, multiple overlaid d, C(C*H*$_3$)$_2$), 0.99–0.95 (12H, b d, C(C*H*$_3$)$_2$), 0.45, 0.41 (3H, d, $^3J_{HH}$ = 6.85 Hz, CH(C*H*$_3$)$_2$). $^{13}C\{^1H\}$ NMR (d_8–Tol, 125.76 MHz): δ 170.2, 168.8 (O*C*(H)N), 166.6 (N*C*(CH_3)CH), 151.1, 145.9, 143.6, 142.3, 141.9, 141.4, 140.8, 125.5, 124.4, 124.3, 124.2, 123.7, 123.2 (*C*–Ar), 94.9 (NC(CH_3)*C*H), 77.9 (O*C*(CH_3)$_2$), 32.4, 28.7, 28.0, 27.7, 27.1, 26.2, (N*C*H(CH_3)$_2$), 26.0 (O*C*(CH_3)$_2$), 25.6, 25.2, 24.8, 24.7, 24.0, 23.4, 22.9 (CH(*C*H_3)$_2$). ^{11}B NMR (d_8–Tol, 125.76 MHz): δ 2.9 H*B*pin. Accurate microanalytical data could not be obtained for this compound.

Magnesium and calcium formamidate hydrodeoxygenation

A solution of compound **4** or **11** (30 mg, 0.067 or 0.056 mmol) in 0.5 ml toluene and two equivalents of a secondary amine were mixed in a J. Young tube. The solution was then interrogated by NMR to ensure complete conversion to the corresponding amide. The solution was then freeze–thaw degassed and exposed to ~1 atm. of CO and the reaction followed by was NMR until complete conversion to the formamidate product. Two equivalents of pinacolborane (0.134 or 0.112 mmol) were then added and the reaction was monitored by ^{1}H, $^{13}C\{^1H\}$ and ^1H–^{13}C gated NMR spectroscopy. Conversion to the methyl amine product from the reactions with **20**, **21**, **23** and **25** and pinacolborane were identified in comparison to the previously reported NMR data.[65] The methyl amine products from the reactions with compounds **18/19** and **21/24** were identified by the characteristic doublet in the ^{1}H NMR spectra centred *ca.*2 – 3 ppm and the corresponding splitting patterns in the ^1H–^{13}C gated NMR spectra. CH_3*n*-BuN(Bpin): ^{1}H NMR (d_8–Tol, 500 MHz): 2.61 (3H, d, $^1J_{HC}$ = 134.47 Hz, (NC*H*$_3$)). ^1H–^{13}C NMR (d_8–Tol, 125.76 MHz): 33.7 (qt, $^1J_{CH}$ = 134.47 Hz, $^3J_{CH}$ = 4.77 Hz, (CH_2N*C*H_3)). CH_3(PhCH_2CH_2)N(Bpin): ^{1}H NMR (d_8–Tol, 500 MHz): 2.75 (3H, d, $^1J_{HC}$ = 134.01 Hz, (NC*H*$_3$)). ^1H–^{13}C NMR (d_8–Tol, 125.76 MHz): 33.9 (qt, $^1J_{CH}$ = 134.01 Hz, $^3J_{CH}$ = 5.72 Hz, (CH_2N*C*H_3)).

Computational Details. Geometry optimizations were performed using Gaussian09 suite of programs[71] using the Becke's 3-parameter hybrid functional,[72] combined with the non-local correlation functional provided by Perdew/Wang.[73] The 6-311+G(d) all-electron basis set was used for the magnesium and the 6-31G(d,p) for the remaining atoms.[74, 75] All stationary points have been identified for minimum (Nimag=0) or transition states (Nimag=1). Intrinsic Reaction Paths (IRPs)[76] were traced from the various transition structures to obtain the connected intermediates.

X-ray Crystallography. Single Crystal X–ray diffraction data for compounds **10**, **12**, **15** – **21** and **23** - **27** were collected on a SuperNova, EosS2 diffractometer using Cu radiation throughout. The crystals were maintained at 150(2) K during data collection. Using Olex2,[77] the structures were solved with the olex2.solve[78] structure solution program and refined with the ShelXL[79] refinement package using Least Squares minimisation. The asymmetric unit of **10** comprises 2 molecules. The structural model includes

75:25 disorder modelling for C59, C60, C128 and C129 with (respectively) C58A, C60A, C1A and C1B. Some distance and ADP restraints were included in the disordered region, to assist convergence. The asymmetric unit of **12** comprises one molecule of the calcium dimer, and one molecule of hexane. The latter is disordered over 2 proximate sites in a 55:45 ratio. C–C distances were restrained to being similar in the disordered solvent region and isotropic ADP restraints were included for some of the partial occupancy carbons therein, to assist convergence. The asymmetric unit of **15** contains half of one molecule, the remainder being generated via an inversion centre proximate to the alkaline earth contender. H1 was located but ultimately included at a calculated position 1.3 Å from Si1. The phenyl ring based on C37 was refined subject to being disordered over 2 proximate sites in a 55:45 ratio. The minor ring component was treated as a rigid hexagon and the ADPs of all fractional occupancy carbons were restrained, in the final least-squares. A solvent mask (Olex–2) was included to treat a region of disordered guest solvent in the lattice. An allowance for half of a molecule of hexane per asymmetric unit has been made in the formula as presented here. The asymmetric unit of **16** comprises half of a dimer molecule. The remainder can be generated via a crystallographic inversion centre. The asymmetric unit of **17** structure contains 2 molecules of the calcium based dimer and 2 molecules of toluene. Disorder in a 65:35 ratio was modelled for C16, C17, C62, C63, C92 C93, C126 and C127. ADP and distance restraints were included for C–C bonds involving fractional occupancy carbons, to attain a chemically sensible convergence. The asymmetric unit of **18** is constituted by 2 molecules of the magnesium based trimer, 2 molecules of ordered toluene and 2.5 molecules of disordered toluene. The latter was treated via PLATON SQUEEZE, in preference to modelling significant disorder and smearing of the electron density. There was some disorder prevalent in the main structure also. In particular, C62, C63, C185, C186, C187, C217, C218, C219 were disordered over 2 sites in a 50:50 ratio, while C54, C55, C164 and C265 were similarly disordered in a 55:45 ratio. ADP and C–C distance restraints were included, on merit, for fractional occupancy carbons and their associated metrics, to assist convergence. The asymmetric unit of **19** contains one dimer and two crystallographically independent dimer halves. The latter are proximate to inversion centres which serve to generate the remaining dimer portion in each case. Disorder prevailed in some of the pendant moieties in this structure. In particular, fractional occupancy atom pairs C102/C12A, C135/C13A, C127/C1D and C128/C1E represent one whole carbon each, split between 2 sites in respective ratios of 70:30, 70:30, 60:40 and 60:40. C60A–C63A are also disordered with C60B–C63B in a 70:30 quotient while C66A–C68A exhibit a 60:40 split with C66B–C68B. Some N–C and C–C distances were restrained to being similar in disordered regions, and ADP restraints were added, on merit, to help achieve convergence. In compound **20** the asymmetric unit comprises half of a dimer molecule and half of one molecule of solvent (toluene). The remainder of the former is generated via a crystallographic inversions centre. The solvent moiety also lies close to an inversion centre, but a combination of disorder (particularly relating to the methyl group) plus smearing of the electron density in the associated phenyl ring precluded derivation of a sensible disorder model without an overwhelming number of restraints. Thus, the solvent

was ultimately treated with PLATON SQUEEZE, and due allowance made for same in the empirical formula presented herein. A crystallographic inversion centre serves to generate the remainder of the dimer molecule. The asymmetric units of **23** and **24** also each comprise one half of a dimer located proximate to a crystallographic inversion centre which serves to generate the remainder of the molecules in both cases. In **25**, the asymmetric unit contains 1 molecule of the calcium based dimer, one ordered half of a hexane molecule (close to a crystallographic inversion centre with generates the remainder), and another hexane half in which the electron density was quite smeared. This latter moiety was treated via PLATON SQUEEZE. C70 in the main feature is disordered over 2 sites in a 75:25 ratio. C–C distances involving these 2 fractional occupancy carbon atoms were restrained in the final least squares, to abet convergence. Half of a dimer molecule and half of a molecule of benzene constitute the asymmetric unit of **26**, with both moieties located proximate to crystallographic inversion centres which generate the remainders. The asymmetric unit of **27** comprises one molecule of the dimer, 1 molecule of hexane with full occupancy and an additional hexane fragment with an overall occupancy of 80%. The Bpin in the main feature was seen to be disordered over 2 sites in a 65:35 ratio. Chemically equivalent bond distances involving the disordered components were restrained to being similar in order to aid convergence. The boron bound fractional hydrogens were included at calculated positions but with freely refined Uiso values. C85 and C86 in the 80% occupancy solvent moiety were disordered in a 50:50 ratio. The electron density in the region of this guest was a somewhat smeared and, as a consequence, some C–C and ADP restraints were included in order to achieve a chemically sensible refinement.

Associated Content

Supporting Information. The Supporting Information is available free of charge on the ACS Publications website at DOI:XXXX.

NMR spectra and computational data for all compounds (PDF)

X-ray crystallographic details (CIF)

Acknowledgements

We thank University of Bath for provision of a doctoral studentship (MDA) and EPSRC (UK) for funding and Professor F. G. N. Cloke and Dr N. Tsoueas for assistance with the Toepler pump experiments.

Table 1: Single Crystal X–ray Data Parameters for compounds **10**, **12**, **15 - 19**.

	10	**12**	**15**	**16**	**17**	**18**	**19**
Empirical formula	$C_{72}H_{108}Mg_2N_4O_2$	$C_{74}H_{114}Ca_2N_4O_4$	$C_{45}H_{61}CaN_2OSi$	$C_{33}H_{54}CaN_4O_2$	$C_{142}H_{203}Ca_4N_{12}O_6$	$C_{117.75}H_{171}Mg_3N_9O_3$	$C_{136}H_{204}Ca_4N_{12}O_4$
Formula weight	1110.24	1203.85	714.12	578.88	2334.47	1833.56	2231.42
Crystal system	monoclinic	monoclinic	monoclinic	monoclinic	triclinic	triclinic	triclinic
Space group	$P2_1/c$	$I2/a$	$P2_1/n$	$P2_1/n$	P–1	P–1	P–1
a/Å	15.31492(11)	22.1065(3)	13.7508(2)	12.5213(1)	12.3167(2)	16.9200(3)	15.6880(5)
b/Å	22.59972(18)	12.64458(13)	15.0080(2)	14.2721(1)	22.2227(4)	26.0844(5)	20.7648(6)
c/Å	39.3251(4)	53.0432(8)	21.5613(3)	18.8389(2)	25.1147(4)	28.3888(4)	22.7564(6)
α/°	90	90	90	90	90.035(1)	67.212(2)	74.394(2)
β/°	95.2592(8)	101.9948(14)	90.001(1)	95.387(1)	98.119(1)	89.8810(10)	72.719(3)
γ/°	90	90	90	90	90.410(1)	82.1420(10)	77.315(3)
Volume/Å^3	13553.64(19)	14503.3(3)	4449.65(11)	3351.74(5)	6805.1(2)	11425.1(4)	6738.4(4)
Z	8	8	4	4	2	4	2
ρ_{calc} g/cm^3	1.088	1.103	1.066	1.147	1.139	1.066	1.100
μ/mm^{-1}	0.653	1.723	1.708	1.862	1.822	0.630	1.806
F(000)	4864.0	5264.0	1548.0	1264.0	2534.0	4002.0	2432.0
Crystal size/mm^3	0.192×0.167×0.156	0.2050×0.1185×0.0478	0.306 × 0.175 × 0.063	0.191×0.145×0.118	0.237 × 0.198 × 0.175	0.284 × 0.219 × 0.129	0.1694×0.0987× 0.0891
2Θ range for data collection/°	5.796 to 139.666	8.178 to 143.898	7.176 to 147.068	7.784 to 146.826	7.11 to 146.862	5.922 to 147.12	5.97 to 144.044
Reflections collected	87144	54447	63736	25873	54860	91161	56557
Independent reflections	25355 [R_{int} = 0.0222]	14051 [R_{int} = 0.0359]	8938 [R_{int} = 0.0420]	6685 [R_{int} = 0.0313]	26890 [R_{int} = 0.0285]	44927 [R_{int} = 0.0281]	25833 [R_{int} = 0.0294]
Data/restraints/parameters	25355/36/1537	14051/93/835	8938/186/464	6685/0/372	26890/95/1594	44927/140/2417	25833/83/1553
Goodness–of–fit on F^2	1.024	1.038	1.067	1.044	1.032	1.017	1.036
Final R indexes [I>=2σ (I)]	R_1 = 0.0394, wR_2 = 0.0985	R_1 = 0.0562, wR_2 = 0.1427	R_1 = 0.0572, wR_2 = 0.1734	R_1 = 0.0387, wR_2 = 0.0989	R_1 = 0.0516, wR_2 = 0.1389	R_1 = 0.0731, wR_2 = 0.2066	R_1 = 0.0542, wR_2 = 0.1398
Final R indexes [all data]	R_1 = 0.0454, wR_2 = 0.1020	R_1 = 0.0679, wR_2 = 0.1495	R_1 = 0.0641, wR_2 = 0.1804	R_1 = 0.0429, wR_2 = 0.1018	R_1 = 0.0629, wR_2 = 0.1476	R_1 = 0.0871, wR_2 = 0.2214	R_1 = 0.0824, wR_2 = 0.1555
Largest diff. peak/hole / e Å^{-3}	0.51/–0.33	0.48/–0.43	0.86/–0.85	0.40/–0.45	0.81/–0.63	1.34/–0.64	0.66/–0.45

Table 2: Single Crystal X–ray Data Parameters for compounds **20**, **21**, **23 - 27**.

	20	**21**	**23**	**24**	**25**	**26**	**27**
Empirical formula	$C_{69.5}H_{102}Mg_2N_6O_2$	$C_{76}H_{102}Mg_2N_6O_2$	$C_{34}H_{51}N_3OCa$	$C_{76}H_{102}Ca_2N_6O_2$	$C_{82}H_{129}Ca_2N_5O_5$	$C_{40}H_{52}MgN_3O$	$C_{84.8}H_{133.2}BCa_2N_5O_5$
Formula weight	1102.18	1180.25	557.85	1211.79	1345.05	615.15	1393.73
Crystal system	monoclinic	orthorhombic	monoclinic	monoclinic	triclinic	monoclinic	triclinic
Space group	$P2_1/n$	$P2_12_12_1$	$C2/c$	$P2_1/n$	P–1	$P2_1/n$	P–1
a/Å	12.9593(2)	13.40560(10)	21.9505(4)	13.2289(2)	12.3369(3)	13.88039(16)	15.3517(7)
b/Å	14.3504(2)	22.4368(2)	14.60243(19)	19.8454(3)	14.1438(3)	11.90132(12)	15.5044(6)
c/Å	18.5552(3)	22.9956(2)	22.8491(4)	14.1282(2)	24.9534(6)	21.6100(2)	19.1840(6)
α/°	90	90	90	90	100.966(2)	90	85.931(3)
β/°	95.8960(10)	90	113.987(2)	108.7856(17)	91.498(2)	100.0066(11)	76.247(3)
γ/°	90	90	90	90	110.918(2)	90	72.926(4)
Volume/Å^3	3432.48(9)	6916.59(10)	6691.3(2)	3511.53(10)	3971.84(17)	3515.56(7)	4239.8(3)
Z	2	4	8	2	2	4	2
ρ_{calc} g/cm^3	1.066	1.133	1.108	1.146	1.125	1.162	1.092
μ/mm^{-1}	0.651	0.680	1.819	1.774	1.634	0.690	1.544
F(000)	1202.0	2560.0	2432.0	1312.0	1472.0	1332.0	1524.0
Crystal size/mm^3	0.251 × 0.137 × 0.089	0.260 × 0.110 × 0.107	0.18 ×0.158×0.083	0.21 ×0.14 × .103	0.161×0.07 ×0.05	0.461×0.365×0.248	0.187×0.126×0.051
2Θ range for data collection/°	7.804 to 146.934	5.504 to 147.058	7.488 to 139.584	7.966 to 139.608	6.848 to 147.038	7.052 to 139.514	5.964 to 146.968
Reflections collected	25278	58616	21184	11731	31950	22341	33340
Independent reflections	6842 [R_{int} = 0.0341]	13812 [R_{int} = 0.0276]	6258 [R_{int} = 0.0213]	6467 [R_{int} = 0.0260]	15669 [R_{int} = 0.0317]	6584 [R_{int} = 0.0253]	16638 [R_{int} = 0.0439]
Data/restraints/parameters	6842/0/355	13812/0/795	6258/0/364	6467/0/398	15669/7/852	6584/0/417	16638/130/1028
Goodness–of–fit on F^2	1.085	1.030	1.027	1.021	1.012	1.040	1.041
Final R indexes [I>=2σ (I)]	R_1 = 0.0602, wR_2 = 0.1592	R_1 = 0.0293, wR_2 = 0.0753	R_1 = 0.0435, wR_2 = 0.1145	R_1 = 0.0427, wR_2 = 0.1114	R_1 = 0.0460, wR_2 = 0.1146	R_1 = 0.0510, wR_2 = 0.1369	R_1 = 0.0675, wR_2 = 0.1795
Final R indexes [all data]	R_1 = 0.0724, wR_2 = 0.1679	R_1 = 0.0308, wR_2 = 0.0763	R_1 = 0.0454, wR_2 = 0.1161	R_1 = 0.0501, wR_2 = 0.1171	R_1 = 0.0637, wR_2 = 0.1258	R_1 = 0.0557, wR_2 = 0.1411	R_1 = 0.0932, wR_2 = 0.1999
Largest diff. peak/hole / e Å^{-3}	0.69/–0.67	0.19/–0.17	0.74/–0.27	0.74/–0.44	0.50/–0.46	0.77/–0.41	1.03/–0.59

References

1. Beller, M.; Cornils, B.; Frohning, C. D.; Kohlpaintner, C. W., *J. Mol. Cat. a-Chem.* **1995,** *104* (1), 17-85.
2. Brennfuhrer, A.; Neumann, H.; Beller, M., *Angew. Chem. Int. Ed.* **2009,** *48* (23), 4114-4133.
3. Barnard, C. F. J., *Organometallics* **2008,** *27* (21), 5402-5422.
4. Herrmann, W. A.; Cornils, B., *Angew. Chem. Int. Ed.* **1997,** *36* (10), 1048-1067.
5. Franke, R.; Selent, D.; Borner, A., *Chem. Rev.* **2012,** *112* (11), 5675-5732.
6. Agbossou, F.; Carpentier, J. F.; Mortreaux, A., *Chem. Rev.* **1995,** *95* (7), 2485-2506.
7. Breit, B., *Acc. Chem. Res.* **2003,** *36* (4), 264-275.
8. Wu, X. F.; Fang, X. J.; Wu, L. P.; Jackstell, R.; Neumann, H.; Beller, M., *Acc. Chem. Res.* **2014,** *47* (4), 1041-1053.
9. Wu, L. P.; Liu, Q.; Jackstell, R.; Beller, M., *Angew. Chem. Int. Ed.* **2014,** *53* (25), 6310-6320.
10. Hebrard, F.; Kalck, P., *Chem. Rev.* **2009,** *109* (9), 4272-4282.
11. Bohnen, H. W.; Cornils, B., *Adv. Catal., Vol 47* **2002,** *47*, 1-64.
12. Pospech, J.; Fleischer, I.; Franke, R.; Buchholz, S.; Beller, M., *Angew. Chem. Int. Ed.* **2013,** *52* (10), 2852-2872.
13. Brummond, K. M.; Kent, J. L., *Tetrahedron* **2000,** *56* (21), 3263-3283.
14. Gibson, S. E.; Stevenazzi, A., *Angew. Chem. Int. Ed.* **2003,** *42* (16), 1800-1810.
15. Schulz, H., *Appl. Catal. a-Gen.* **1999,** *186* (1-2), 3-12.
16. Herrmann, W. A., *Angew. Chem. Int. Ed. in English* **1982,** *21* (2), 117-130.
17. West, N. M.; Miller, A. J. M.; Labinger, J. A.; Bercaw, J. E., *Coord. Chem. Rev.* **2011,** *255* (7-8), 881-898.
18. Giannini, L.; Caselli, A.; Solari, E.; Floriani, C.; ChiesiVilla, A.; Rizzoli, C.; Re, N.; Sgamellotti, A., Organometallic *J. Am. Chem. Soc.* **1997,** *119* (41), 9709-9719.
19. Fachinetti, G.; Floriani, C.; Roselli, A.; Pucci, S., *J. Chem. Soc.-Chem. Commun.* **1978,** (6), 269-270.
20. Fachinetti, G.; Fochi, G.; Floriani, C., *J. Chem. Soc.-Dalton Trans.* **1977,** (20), 1946-1950.
21. Manriquez, J. M.; McAlister, D. R.; Sanner, R. D.; Bercaw, *J. Am. Chem. Soc.* **1978,** *100* (9), 2716-2724.
22. Manriquez, J. M.; McAlister, D. R.; Sanner, R. D.; Bercaw, J. E., *J. Am. Chem. Soc.* **1976,** *98* (21), 6733-6735.
23. Moloy, K. G.; Fagan, P. J.; Manriquez, J. M.; Marks, T. J., *J. Am. Chem. Soc.* **1986,** *108* (1), 56-67.
24. Fagan, P. J.; Moloy, K. G.; Marks, T. J., *J. Am. Chem. Soc.* **1981,** *103* (23), 6959-6962.
25. Evans, W. J.; Grate, J. W.; Doedens, R. J., *J. Am. Chem. Soc.* **1985,** *107* (6), 1671-1679.

26. Cummins, C. C.; Vanduyne, G. D.; Schaller, C. P.; Wolczanski, P. T., *Organometallics* **1991,** *10* (1), 164-170.
27. Ferrence, G. M.; McDonald, R.; Takats, J., *Angew. Chem. Int. Ed.* **1999,** *38* (15), 2233-2237.
28. Werkema, E. L.; Maron, L.; Eisenstein, O.; Andersen, R. A., *J. Am. Chem. Soc.* **2007,** *129* (9), 2529-2541.
29. Trzupek, L. S.; Newirth, T. L.; Kelly, E. G.; Sbarbati, N. E.; Whitesides, G. M., *J. Am. Chem. Soc.* **1973,** *95* (24), 8118-8133.
30. Ryang, M.; Rhee, I.; Tsutsumi, S., *Bull. Chem. Soc. Japan* **1964,** *37* (3), 341-343.
31. Ryang, M.; Tsutsumi, S., *Nippon Kagaku Zasshi* **1961,** *82* (7), 880-882.
32. Ryang, M.; Tsutsumi, S.; Miyamoto, H., *Nippon Kagaku Zasshi* **1961,** *82* (9), 1276-1278.
33. Jutzi, P.; Schroder, F. W., *Angew. Chem. Int. Ed.* **1971,** *10* (5), 339.
34. Jutzi, P.; Schroder, F. W., *J. Organometal. Chem.* **1970,** *24* (1), 1-5.
35. Jutzi, P.; Schroder, F. W., *J. Organometal. Chem.* **1970,** *24* (3), C43-C44.
36. Orita, A.; Fukudome, M.; Ohe, K.; Murai, S., *J. Org. Chem.* **1994,** *59* (2), 477-481.
37. Orita, A.; Ohe, K.; Murai, S., *Organometallics* **1994,** *13* (4), 1533-1536.
38. Perez, D. G.; Nudelman, N. S., *J. Org. Chem.* **1988,** *53* (2), 408-413.
39. Nudelman, N. S.; Perez, D., *Anal. Asoc. Quim. Argentina* **1981,** *69* (4), 195-204.
40. Rautenstrauch, V.; Joyeux, M., *Angew. Chem. Int. Ed. Engl.* **1979,** *18* (1), 83-85.
41. Rautenstrauch, V.; Joyeux, M., *Angew. Chem. Int. Ed. Engl.* **1979,** *18* (1), 85-86.
42. Narayana, C.; Periasamy, M., *Synthesis-Stuttgart* **1985,** (3), 253-268.
43. Anker, M. D.; Hill, M. S.; Lowe, J. P.; Mahon, M. F., *Angew. Chem. Int. Ed.* **2015,** *54* (34), 10009-10011.
44. Lalrempuia, R.; Kefalidis, C. E.; Bonyhady, S. J.; Schwarze, B.; Maron, L.; Stasch, A.; Jones, C., *J. Am. Chem. Soc.* **2015,** *137* (28), 8944-8947.
45. Bonyhady, S. J.; Jones, C.; Nembenna, S.; Stasch, A.; Edwards, A. J.; McIntyre, G. J., *Chem. Eur. J.* **2010,** *16* (3), 938-955.
46. Harder, S.; Brettar, J., *Angew. Chem. Int. Ed.* **2006,** *45* (21), 3474-3478.
47. Harder, S., *Organometallics* **2002,** *21* (18), 3782-3787.
48. Jochmann, P.; Davin, J. P.; Spaniol, T. P.; Maron, L.; Okuda, J., *Angew. Chem. Int. Ed.* **2012,** *51* (18), 4452-4455.
49. Ragaini, F., *Dalton Trans.* **2009,** (32), 6251-6266.
50. Allen, C. L.; Williams, J. M. J., *Chem. Soc. Rev.* **2011,** *40* (7), 3405-3415.
51. Gerack, C. J.; McElwee-White, L., *Molecules* **2014,** *19* (6), 7689-7713.
52. Fox, D. J.; Bergman, R. G., *Organometallics* **2004,** *23* (8), 1656-1670.
53. Fox, D. J.; Bergman, R. G., *J. Am. Chem. Soc.* **2003,** *125* (30), 8984-8985.
54. Nudelman, N. S.; Perez, D. G., *J. Chem. Soc. Perkin Trans. 2* **1989,** (8), 931-936.

55. Furlong, J. J. P.; Lewkowicz, E. S.; Nudelman, *J. Chem. Soc. Perkin Trans. 2* **1990,** (8), 1461-1465.
56. Viruelamartin, P.; Viruelamartin, R.; Tomas, F.; Nudelman, N. S., *J. Am. Chem. Soc.* **1994,** *116* (22), 10110-10116.
57. Hilf, C.; Bosold, F.; Harms, K.; Lohrenz, J. C. W.; Marsch, M.; Schimeczek, M.; Boche, G., *Chem. Ber.* **1997,** *130* (9), 1201-1212.
58. Boche, G.; Hilf, C.; Harms, K.; Marsch, M.; Lohrenz, J. C. W., *Angew. Chem. Int. Ed. Engl.* **1995,** *34* (4), 487-489.
59. Nudelman, N. S.; Doctorovich, F.; Linares, G. G.; Schulz, H.; Mendiara, S., *Gazz. Chim. Ital.* **1996,** *126* (1), 19-24.
60. Ruspic, C.; Harder, S., *Inorg. Chem.* **2007,** *46* (24), 10426-10433.
61. Aljuaid, S. S.; Eaborn, C.; Hitchcock, P. B.; Kundu, K.; McGeary, C. A.; Smith, J. D., *J. Organometal. Chem.* **1994,** *480* (1-2), 199-203.
62. Avent, A. G.; Crimmin, M. R.; Hill, M. S.; Hitchcock, P. B., *Dalton Trans.* **2004,** (20), 3166-3168.
63. Barrett, A. G. M.; Casely, I. J.; Crimmin, M. R.; Hill, M. S.; Lachs, J. R.; Mahon, M. F.; Procopiou, P. A., *Inorg. Chem.* **2009,** *48* (10), 4445-4453.
64. Avent, A. G.; Crimmin, M. R.; Hill, M. S.; Hitchcock, P. B., *Dalton Trans.* **2005,** (2), 278-284.
65. Yang, Y.; Anker, M. D.; Fang, J.; Mahon, M. F.; Maron, L.; Weetman, C.; Hill, M. S., *Chemical Science* **2017**, *8*, 3529-3537.
66. Barrett, A. G. M.; Crimmin, M. R.; Hill, M. S.; Kociok-Köhn, G.; MacDougall, D. J.; Mahon, M. F.; Procopiou, P. A., *Organometallics* **2008,** *27* (15), 3939-3946.
67. Turner, Z. R.; Buffet, J. C., *Dalton Trans.* **2015,** *44* (29), 12985-12989.
68. Arrowsmith, M.; Hill, M. S.; MacDougall, D. J.; Mahon, M. F., *Angew. Chem. Int. Ed.* **2009,** *48* (22), 4013-4016.
69. Weetman, C.; Hill, M. S.; Mahon, M. F., *Chem. Eur. J.* **2016,** *22* (21), 7158-7162.
70. Liptrot, D. J.; Hill, M. S.; Mahon, M. F.; Wilson, A. S. S., *Angew. Chem. Int. Ed.* **2015,** *54* (45), 13362-13365.
71. Frisch, M. J.; Trucks, G. W.; Schlegel, H. B.; Scuseria, G. E.; Robb, M. A.; Cheeseman, J. R.; Scalmani, G.; Barone, V.; Petersson, G. A.; Nakatsuji, H.; Li, X.; Caricato, M.; Marenich, A. V.; Bloino, J.; Janesko, B. G.; Gomperts, R.; Mennucci, B.; Hratchian, H. P.; Ortiz, J. V.; Izmaylov, A. F.; Sonnenberg, J. L.; Williams; Ding, F.; Lipparini, F.; Egidi, F.; Goings, J.; Peng, B.; Petrone, A.; Henderson, T.; Ranasinghe, D.; Zakrzewski, V. G.; Gao, J.; Rega, N.; Zheng, G.; Liang, W.; Hada, M.; Ehara, M.; Toyota, K.; Fukuda, R.; Hasegawa, J.; Ishida, M.; Nakajima, T.; Honda, Y.; Kitao, O.; Nakai, H.; Vreven, T.; Throssell, K.; Montgomery Jr., J. A.; Peralta, J. E.; Ogliaro, F.; Bearpark, M. J.; Heyd, J. J.; Brothers, E. N.; Kudin, K. N.; Staroverov, V. N.; Keith, T. A.; Kobayashi, R.; Normand, J.; Raghavachari, K.; Rendell, A. P.;

Burant, J. C.; Iyengar, S. S.; Tomasi, J.; Cossi, M.; Millam, J. M.; Klene, M.; Adamo, C.; Cammi, R.; Ochterski, J. W.; Martin, R. L.; Morokuma, K.; Farkas, O.; Foresman, J. B.; Fox, D. J. *Gaussian 16*, Wallingford, CT, 2016.

72. Becke, A. D., *J. Chem. Phys.* **1993,** *98* (7), 5648-5652.
73. Perdew, J. P.; Wang, Y., *Phys. Rev. B* **1992,** *45* (23), 13244-13249.
74. McLean, A. D.; Chandler, G. S., *J. Chem. Phys.* **1980,** *72* (10), 5639-5648.
75. Hehre, W. J.; Ditchfield, R.; Pople, J. A., *J. Chem. Phys.* **1972,** *56* (5), 2257-+.
76. Gonzalez, C.; Schlegel, H. B., *J. Chem. Phys.* **1989,** *90* (4), 2154-2161.
77. Dolomanov, O. V.; Bourhis, L. J.; Gildea, R. J.; Howard, J. A. K.; Puschmann, H., *J. Appl. Crystallogr.* **2009,** *42*, 339-341.
78. Bourhis, L. J.; Dolomanov, O. V.; Gildea, R. J.; Howard, J. A. K.; Puschmann, H., *Acta Cryst. a-Found. Adv.* **2015,** *71*, 59-75.
79. Sheldrick, G. M., *Acta Cryst. C-Struct. Chem.* **2015,** *71*, 3-8.

For Table of Contents entry